The Pennsylvania State University

The Graduate School

SLIPS-LAB FOR URINARY STONE DIAGNOSTICS

A Dissertation in

Bioengineering

by

Hui Li

Submitted in Partial Fulfillment
of the Requirements
for the Degree of

Doctor of Philosophy

August 2019

The dissertation of Hui Li was reviewed and approved* by the following:

Pak Kin Wong
Professor of Biomedical Engineering
Dissertation Advisor
Committee Chair

Tak Sing Wong
Assistant Professor of Biomedical Engineering

Siyang Zheng
Assistant Professor of Biomedical Engineering

Lauren Zarzar
Assistant Professor of Chemistry

William Hancock,
Professor of Biomedical Engineer
Chair of the Graduate Program

*Signatures are on file in the Graduate School

ABSTRACT

Urinary stone disease, or kidney stones, affects ~19% of men and 9% of women during their lifetime and carries a $5 billion annual healthcare expenditure. Current guidelines recommend metabolic workup based on 24-hour urine collection for high risk stone formers to identify potential underlying etiologies, initiate dietary and pharmacologic interventions, and their therapeutic monitoring. The slow, expensive, and inconvenient steps hinder routine monitoring and delivery of optimal care. In this study, we develop the SLIPS-LAB, a cellphone-sized POC medical system, for rapid measurement of urinary stone analytes to facilitate management of high-risk urinary stone patients. The SLIPS-LAB is designed using a biologically inspired liquid-repellent surfaces, Slippery Liquid-Infused Porous Surface (SLIPS). The ultrarepellent surface allows autonomous droplet manipulation with zero-power requirement. The non-fouling property of SLIPS enables manipulation of analytical fluids (e.g., water, milk, and honey) and physiological fluids (e.g., urine, blood, saliva, and plasma) and prevents loss of target analytes. Sample preparation procedures including volume metering, reagent mixing, and reaction time control can be automated by properly designing the system. Similar to blood glucose monitoring, the simplicity and speed of SLIPS-LAB hold the potential to provide actionable diagnostic information for patients with urinary stone disease and improve their adherence to dietary and pharmacologic treatments. To validate the clinical feasibility of the prototype SLIPS-LAB, we pilot a study of examining the urinary stone related metabolic workups for 15 urine samples from patients. The results suggest high coordination with clinical reports.

TABLE OF CONTENTS

LIST OF FIGURES vii

ACKNOWLEDGEMENTS x

Chapter 1 Introduction 1

1.1 Urinary stone disease is a big challenge to human beings 1

1.2 Current guidelines for urinary stone diagnostics 2

1.3 The SLIPS-LAB for advancing the urinary stone management 4

Chapter 2 Design of the SLIPS-LAB for point-of-care diagnostics 6

2.1 Materials and methods 6

2.1.1 Fabrication for the SLIPS-LAB 7

2.1.2 Zero-power fluid transportation on SLIPS-LAB 8

2.1.3 Quantitative study of the sampling process 9

2.1.4 Quantitative study of the loading process 10

2.2 Results and discussions 11

2.2.1 Slippery Liquid-Infused Porous Surface engineered Lab (SLIPS-LAB) for urinary stone diagnostics 11

2.2.2 Design of the SLIPS-LAB 14

Chapter 3 Detection of stone related metabolic workups on the SLIPS-LAB 19

3.1 Materials and methods 19

3.1.1 Design of the SLIPS-LAB for multiplex detection 20

3.1.2 Characterization of detecting urinary stone-related metabolic workups 20

3.1.3 Pre-clinical study of detecting urine from a volunteer 22

3.2 Results and discussions 22

3.2.1 Design of the SLIPS-LAB for multiplex detection 22

3.2.2 Colorimetric detection of urinary stone related metabolic workups on the SLIPS-LAB 25

Chapter 4 Urinary stone diagnostics for clinical samples 28

4.1 Materials and methods 28

4.1.1 Clinical study of detecting urine directly from patients 29

4.1.2 Statistical analysis 29

4.2 Results and discussions 29

4.2.1 Clinical study of detecting urine directly from patients 30

4.2.2 Personalized treatment for patients at risk of urinary stone 32

Chapter 5 Conclusion and future work 34

References 37

Appendix A Supplementary materials for Chapter 2 42

Appendix B Supplementary materials for Chapter 3 55

Appendix C Supplementary materials for Chapter 4 64

LIST OF FIGURES

Figure 1-1. Current workflow for metabolic evaluation of patients with urinary stone disease. Current guidelines recommend 24-hour urine collection for high risk stone formers. The patient collects all urine within the 24-hour period (~ 2 liters) in a bulky container and kept cool, either on ice or in a refrigerator. After completion, the urine sample is sent to a centralized laboratory (usually in a different state) for detecting the relevant urinary analytes, such as calcium, citrate, urate, oxalate, pH, sodium, and sulfate. The results, along with a risk analysis report, are available for the physician in approximately 1-2 weeks after collection. In certain clinical scenarios, a second collection may be recommended. The proposed SLIPS-LAB will enable testing either in the clinic setting or at home, and significantly improve the efficiency of monitoring dietary and pharmacologic treatments. 3

Figure 2-1: **Slippery Liquid-Infused Porous Surface engineered Lab (SLIPS-LAB) for point-of-care diagnostics.** (**a**) Overview of urinary stone diagnostics using SLIPS-LAB. Diagnostics was demonstrated using the SLIPS-LAB in a clinical study and compared with the clinical report. (**b**) The SLIPS-LAB achieves sampling, zero-power loading, and detection processes in a point-of-care manner. Analyte can be sampled, transported on the SLIPS material, and detected using colorimetric assays. (**c**) The SLIPS-LAB is

capable of managing various of viscous fluids and biological fluids. Images are representative for at least two independent experiments. Scale bar, 5 mm. 13

Figure 2-2: **Design of the SLIPS-LAB.** (**a**) The SLIPS-LAB can implement accurate sampling, zero-powered loading, tunable loading time, and mixing in one device. Images are representative for two independent experiments. Scale bar, 2 mm. (**b-c**) Mechanism of sampling liquid at the large and small volume, respectively. (**d**) Mechanism of the zero-powered loading process. The feasibility of tuning loading time can be demonstrated. (**e-f**) Mechanism of leading the samples into the reaction chamber and the mixing process. (**g-h**) Quantitative analysis of the sampling for large and small volume range, respectively. The data represent mean ± SEM. Each data point was collected from 10-30 independent tests. (**i**) Quantitative analysis of tuning the loading time using different designs. The data represent mean ± SEM. Each data point was collected from 10-20 independent tests. 17

Figure **3-1. SLIPS-LAB for multiplex detection.** (**a-c**) The engineering design of the SLIPS-LAB for multiplex detection. Scale bar, (a) and (b), 5 mm; (c) 1 mm. (**d**) Demonstration for multiplex detections, including sample loading, time control, and mixing for detection. Images are representative for two independent experiments. (**e**) The design of SLIPS-LAB to perform the colorimetric assays to test the urinary stone related metabolic workups..... 24

Figure **3-2. Demonstration of urinary stone diagnostics using the SLIPS-LAB.** (**a**) Calibration of the colorimetric assays for respective metabolic ions. Different color represents respective color element in the test. The data represent mean ± SEM (n= 3). (**b**) Urinary stone diagnostics on the SLIPS-LAB for a urine sample from a volunteer and the comparison with the results from standard methods. The data represent mean ± SEM (n= 3 using SLIPS-LAB and n= 2 using standard methods). 27

Figure 4-1. Clinical validation of the SLIPS-LAB for urinary stone diagnosis. (**a**) The procedures of performing urinary stone diagnostics using SLIPS-LAB. (**b**) Linear regression of the diagnostic results for each workup from the SLIPS-LAB and the clinical reports. The data represent mean ± SEM (n= 3). (**c**) Bland–Altman plot of the diagnostic results to better assess the trend, the spot outliers, and the magnitude of disagreement between the SLIPS-LAB and the clinical reports. 31

Figure **4-2. Personalized treatment for patients at risk of urinary stone.** Urinary stone risk for individuals, including (**a**) the healthy case and (**b-d**) the high-risk cases with distinct stone formation mechanisms. 33

ACKNOWLEDGEMENTS

To date, it comes to the end of my Phd training. I appreciate people who have helped me in the past 5 years. It is impossible to complete my training without their help.

I would like to thank my committee members, including Prof. Pak Kin Wong, Prof. Tak Sing Wong, Prof. Siyang Zheng, and Prof. Lauren Zarzar, for their guidance and support. I am grateful for their valuable insights and suggestions. In particular, I expect to express my gratitude and appreciation to my supervisor, Prof. Pak Kin Wong, for his guidance for the research work I have conducted in my training. He has initialized research topics, overseen experimental details, and launched valuable discussions. These experiences are priceless in my life. Furthermore, his hard working motivates me every day in my study and forever in the future.

I would like to acknowledge the collaborators for their considerable contribution and valuable insights, including Prof. Joseph C. Liao, Dr. Kathleen E. Mach, and MD. Eugene Shkolyar at Stanford University, Prof. Tak Sing Wong, Prof. Francisco Diaz, Dr. Jing Wang, and Mr. Tyler Garner at Penn State University, Prof. Neal J. Thomas, Prof. David W. Craft, and Dr. Matthew R. England at Penn State Milton S. Hershey Medical Center, Dr. Chris Puleo and Dr. Christine Surrette at GE Global Research. I appreciate their inputs to make the research work happen.

I would like to thank our lab members, including Dr. Jian Gao, Dr. Shue Wang, Dr. Yuan Xiao, Dr. Yongliang Yang, Dr. Zach Dean, Dr. Nima Jamilpour, Dr. Sun Jian, Dr. Yi Lu, Dr. Tingting Liu, Dr. Ying Wan, Peter Torab, Samuel Vilchez, Eric Ninghao Zhu,

Yue Yan, Tyler Malcom, Britney Forsyth, and Sara Korsunsky. They have built up a great academic environment. I appreciate the valuable discussion, interesting ideas, and leisure activities we have together.

I would like to thank all my friends for the encouragement and discussion during my study, which is of importance to lead me forward.

I appreciate the supports from my wife, my daughter, my parents, my brother, and other family members. Without their understanding and support, it is impossible to finish my PhD study.

Lastly, I acknowledge the Pennsylvania State University and the Department of the Biomedical Engineering for the opportunity of letting me pursuit my study.

Chapter 1

Introduction

In this chapter, we will descript the urinary stone disease and the challenges caused by this disease. The mechanisms leading to the urinary stone disease will be discussed to understand the potentials to relieve this challenge. In particular, advanced diagnostics will be considered as one of the most effective strategies to benefit the urinary stone management in clinical. We will propose the potential of developing a novel medical device for urinary stone diagnostics using a bio-inspired material, namely the Slippery Liquid-infused Porous Surface (SLIPS). The advantages of the SLIPS will be explained in detail.

1.1 Urinary stone disease is a big challenge to human beings

Urinary (kidney) stones are solid materials formed in the urinary, which are typically resulting from the concentrated metabolic products that allow the crystallization of the minerals and the accumulation of the minor crystals [1, 2]. The lifetime incidence of urinary stones is 11% in men and 9% in women [3-5]. In the U.S., urinary stone disease accounts for two million annual outpatient visits and 200,000 hospital stays, contributing towards an overall healthcare expenditure estimated between $2 to 5 billion [4-6]. The global urinary stone burden is increasing steadily due to aging population, rising incidence of obesity, diabetes, and hypertension [7-9]. The recurrence rate of urinary stone is as high

as 60-80%, highlighting the importance of preventative efforts [10-12]. The dimensions of the stones vary from submillimeter to tens of millimeters. While it can be extremely debilitating and severely stressful, most small stones pass spontaneously and are managed non-surgically with hydration and pain control [13, 14]. Larger stones can be lodged in the urinary tract, which can cause urinary tract obstruction, recurrent infections, and require urologic intervention via lithotripsy [15-19]. As prolonged urinary tract obstruction leads to urinary injury and other morbidity, high risk stone formers are recommended to undergo a metabolic workup to identify etiologic factors and guide possible dietary and pharmacologic interventions, typically under the supervision of a urologist or a nephrologist [20, 21].

1.2 Current guidelines for urinary stone diagnostics

Common urinary stone types include calcium oxalate, calcium, phosphate, uric acid, and struvite [22, 23]. In addition to chemical analysis of stone composition, the American Urological Association Medical Management of Urinary Stones Guidelines recommend a 24-hour urine collection for high risk stone formers to identify potential underlying etiologies, initiate dietary and pharmacologic interventions, and their therapeutic monitoring [24, 25]. The test includes a measurement of urine volume, pH, oxalate, urate, citrate, sodium, potassium and creatinine [26]. Currently, urine collection is typically done using a commercial kit (e.g., Litholink and UroRisk), kept cool and shipped to a centralized clinical laboratory to measure the urinary analytes (**Figure 1-1**). A risk analysis is available for physicians in approximately 1-2 weeks and a second collection

may be recommended in certain scenarios. Despite being recommended by multiple guidelines, the current practice grossly hinder routine monitoring and delivery of optimal care due to the high testing cost, cumbersome collection procedures, and long delay in

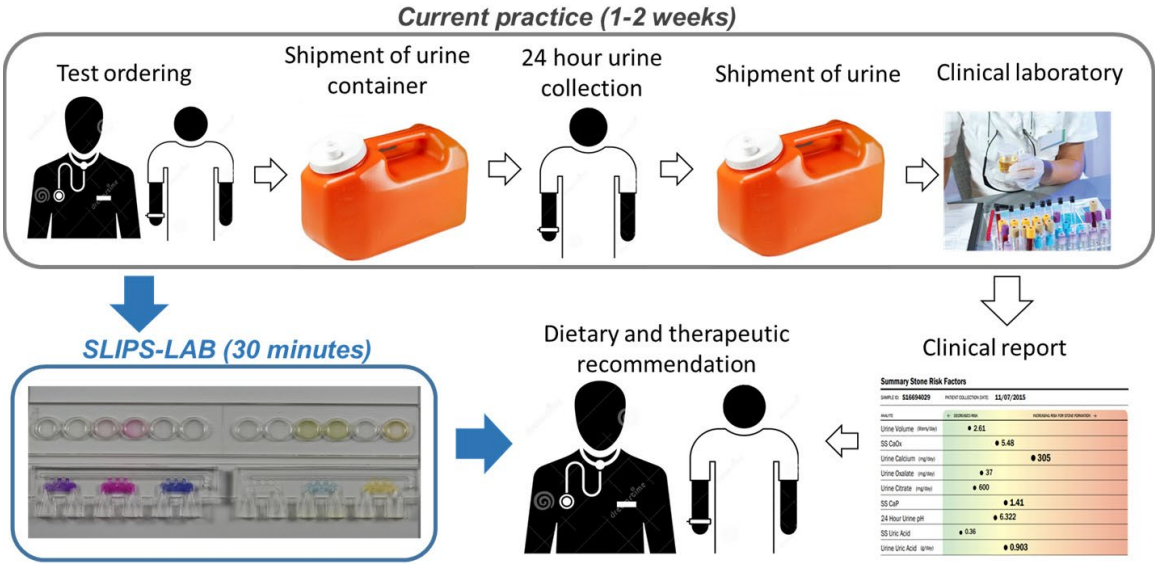

Figure 1-1. Current workflow for metabolic evaluation of patients with urinary stone disease. Current guidelines recommend 24-hour urine collection for high risk stone formers. The patient collects all urine within the 24-hour period (~ 2 liters) in a bulky container and kept cool, either on ice or in a refrigerator. After completion, the urine sample is sent to a centralized laboratory (usually in a different state) for detecting the relevant urinary analytes, such as calcium, citrate, urate, oxalate, pH, sodium, and sulfate. The results, along with a risk analysis report, are available for the physician in approximately 1-2 weeks after collection. In certain clinical scenarios, a second collection may be recommended. The proposed SLIPS-LAB will enable testing either in the clinic setting or at home, and significantly improve the efficiency of monitoring dietary and pharmacologic treatments.

obtaining the results [27, 28]. Unlike blood glucose monitoring for diabetic patients and other home health monitoring systems, rapid diagnostic tests for urinary stone disease is undeveloped and a point-of-care testing device is not available**.** Current strategies for urinary stone prevention do not use spot urine testing because it is typically performed only once during the day and then sent to a clinical laboratory for analysis [29, 30]. This delay in turnaround time precludes real-time feedback for successful adherence to dietary or medication dosing regimen [31]. Isolated spot urine testing is also inferior to 24-hr urine testing because a single spot urine can be heavily influenced by food ingestion and hydration status and thus cannot serve as a surrogate for integrated daily stone risk [32]. There is an urgent need to develop point-of-care (POC) medical technologies for performing metabolic evaluation for the high-risk populations (e.g., recurrent stone formers, patients with personal and family history, obesity, high blood pressure, and medication) and for improving patient compliance to diet, medications and treatments.

1.3 The SLIPS-LAB for advancing the urinary stone management

In this study, we develop the SLIPS-LAB, a cellphone-sized POC medical system, for rapid measurement of urinary stone analytes to facilitate management of high-risk urinary stone patients. This standalone biochemical analysis system is built on a biologically inspired liquid-repellent surfaces, Slippery Liquid-Infused Porous Surface (SLIPS) [33]. The ultrarepellent surface allows autonomous droplet manipulation with zero-power requirement. The non-fouling property of SLIPS enables manipulation of bodily fluids such as urine, blood, saliva, trachea sample, and plasma, and prevents loss of

target analytes. Sample preparation procedures can be automated on the system, including volume metering, reagent mixing, and reaction time control. Similar to blood glucose monitoring, the simplicity and speed of SLIPS-LAB hold the potential to provide actionable diagnostic information for patients with urinary stone disease and improve their adherence to dietary and pharmacologic treatments. The clinical feasibility of the prototype SLIPS-LAB has been validated in a pilot study in which the urinary stone related metabolic workups are detected for 15 urine samples from patients. High coordination between the SLIPS-LAB and the clinical reports has been demonstrated.

Chapter 2

Design of the SLIPS-LAB for point-of-care diagnostics

In this chapter, we will introduce a Slippery Liquid-Infused Porous Surface engineered lab (SLIPS-LAB) for point-of-care (POC) diagnostics and specially the application to advance the urinary stone diagnostics. The materials, the fabrication process, the study design, and the experimental details of the SLIPS-LAB will be descripted. The performance of the SLIPS-LAB for wide applications will be elucidated by demonstrating the capability of managing various of analytical fluids and physiological fluids. The physical models and the experimental demonstrations for achieving the feature capabilities of the SLIPS-LAB will be interpreted step by step, including the accurate sampling, zero-powered sample loading, and automatic mixing processes. Necessary discussions will be included as well.

2.1 Materials and methods

In this section, we will list the materials required to fabricate the SLIPS-LAB and explain the details of the fabrication processes and calibration processes. This section includes four part: the fabrication for the SLIPS-LAB, the demonstration of the zero-powered fluid transportation on the SLIPS-LAB, the quantitative study of the sampling process, as well as the quantitative study of the loading process.

2.1.1 Fabrication for the SLIPS-LAB

Polydimethylsiloxane (PDMS) (Sylgard 184) for device fabrication was obtained from Dow Corning. The oil for surface treatment was hydroxy terminated polydimethylsiloxane (Sigma Aldrich, 481939). Acrylic sheets for fabricating the device mold were from McMaster-Carr and ePlastics. The thickness were 0.76 mm, 1.51 mm, and 3.02 mm in different designs. Two lyaers of acrylic sheets were patterned using a laser machining system (Universal Laser Systems) to create the mold for the soft lithography process. The bottom layer consisted of the converging loading legs, reaction chambers, the air channel, and the connecting channels between reaction chambers and the air channel. The top layer consisted of the converging loading legs. The two layers were aligned and bonded together using a layer of double-sided tape (3M) to create a 3D mold. Liquid PDMS (at ratio of 10:1 between pre-polymer and cross-linker) was poured on the mold and cured for 3 hr at 80°C. The thickness of the PDMS layer was determined by dividing the weight of the applied PDMS of the density of the PDMS and the surface area of the substrate. The PDMS was peeled off from the mold. Holes were punched in the reaction chambers using punches at the inner diameter of 1.5 mm, 2.0 mm, and 3.0 mm (Ted Pella, Inc. and Harris Uni-Core). The diameter, number, and location of the holes were determined according to the designs. Another PDMS layer was prepared by pouring liquid PDMS (at ratio of 10:1 between pre-polymer and cross-linker) on a bare glass slide and curing for 3 hr at 80°C. The thickness of this layer was 1 mm. Both the PDMS layers were cleaned with ethanol three time and DI water once. The two layers were subsequently bonded together after 5 min air plasma treatment (PDC-001, Harrick Plasma). The device

was incubated for 1 hr at 80°C. The device was treated in a hydroxy terminated PDMS bath at 55°C overnight. Extra hydroxy terminated PDMS was dumped out after this process. The device was bonded with a glass slide or a laser machined acrylic sheet using a double-sided tape.

2.1.2 Zero-power fluid transportation on SLIPS-LAB

Zero-power fluid transportation was demonstrated for two types of fluids, including analytical fluids and physiological fluids. **Viscous fluids:** Distilled water was used throughout the study unless otherwise specified. The food dye, milk (1%), juice (100% grape juice), syrup (Combs Family Farms), and honey (100% pure honey, Buckwheat, Weis) were from grocery store. The glycerol was from Fisher Bioreagents (153421). **Biological fluids:** Urine was collected from a healthy volunteer and stored at 4 degree Celsius to demonstrate the sample loading on SLIPS-LAB (collected at 7:30 pm on 10/24/18). Saliva was freshly collected from a healthy volunteer for demonstration. Human whole blood samples were obtained from BioIVT. Citrate phosphate dextrose (CPD) was applied as the anticoagulant. The plasma was isolated from the whole blood using a centrifuge protocol, which was 200 g for 20 min. The tracheal aspirate (TA) was from a patient admitted at the Penn State Milton S. Hershey Medical Center.

All samples were loaded at the entrance of the SLIPS-LAB when the SLIPS-LAB was tilted down at an angle of ~ 45°. The volume was 45 μL. A piece of tape was well bonded on the hole of the air channel. The device was flattened on a table. The zero-power fluid transportation happened when the tape was unsealed. Owing to the 3D channel design,

the samples were automatically loaded into the reaction chambers and mixed together. The process was monitored using a digital camera (Nikon AF-S Micro Nikkor 105 mm, Nikon D750).

2.1.3 Quantitative study of the sampling process

Two scenarios were designed to sample liquid samples in a large range volume. The converging loading legs were dipped in liquid to sample the liquid in large volumes (e.g., 10-50 μL). Briefly, the loading legs were dipped in the liquid (i.e, water) where the depth of the liquid was determined by the volume of the liquid divided by the surface area of the container (i.e., Petri dish, 30-2041). The loading legs were pulled out from the liquid when the air channel was sealed with a piece of tape. The liquid was pipetted out after unsealing the air channel. The mass was individually measured on a precise weight scale (XS205, Mettler Toledo) and the volume was calculated by the mass divided by the density of the liquid. The sample volume was also studied with devices at different thickness, which was tuned by the thickness of the initial mold, by replicating the above protocols.

To sample liquid in small volumes (e.g., 1-10 μL), holes were engineered to retain the liquid passing through. A piece of tissue paper (Kimtech Science, 05511) was held with a tweezer. The paper was able to reserve liquid and lead the liquid passing through the holes. This protocol was straightforward and replicable that was also achieved by using a pipette to hold the liquid and pass through the holes (**Supplementary Movie S2-2**). The liquid in the holes were pipetted out and the mass was measured on the precise weight scale. To note, the samples in relatively large volume (i.e., > 2 μL) were individually

measured; whereas the samples in extremely small volume (i.e., < 2 μL) were measured by averaging 3 samples collected together. The volume was calculated by the mass divided by the density of the liquid. The sample volume was studied with holes at different diameter and different thickness (measured using a caliper), which were engineered by the punch and the device thickness, by replicating the above protocols.

2.1.4 Quantitative study of the loading process

The zero-power loading process was quantitatively studied. The relationship between the loading speed and the converging angle and the thickness of the loading legs was built up. In the experiment, the converging angle of the loading legs ranged from 0° to 20° with an interval of 5° and the thickness of the loading legs was 0.75 mm, 1.5 mm, and 3.0 mm. In this experiment, the mold of the device consisted of the converging loading legs and the air channel on a single layer (i.e., the bottom layer as mentioned). The length of the loading legs was 1.5 cm, which was the vertical distance between the loading entrance and the inner edge of the air channel. The liquid was sampled as described above. The device was flattened on a table. The loading was initialized when the air channel was unsealed. The process was monitored using the mentioned digital camera. The loading time was defined as the time frame between the air channel was unsealed and the sample reach the air channel. The movie was 10 min in total. The unsuccess loading within this time frame would not be analyzed or presented in data analysis section. We neglected the extremely slow loading process, which could be significantly affected by minor errors,

such as the fabrication. An alternative was designed to achieve the extremely slow loading process, which would be explained in the discussion section.

2.2 Results and discussions

In this section, we will introduce the study design of applying the SLIPS-LAB for POC diagnostics (e.g., urinary stone diagnostics), explain the experimental results for demonstrating the performance of the SLIPS-LAB for wide applications, and investigate the theoretical analysis and respective experimental results to uncover the functionalization the SLIPS-LAB. In particular, the performance of the SLIPS-LAB for wide applications will be demonstrated by managing analytical fluids and physiological fluids. The physical models and the experimental demonstrations to functionalize the feature capabilities of the SLIPS-LAB will be detailed step by step, including the accurate sampling, zero-powered sample loading, and automatic mixing processes.

2.2.1 Slippery Liquid-Infused Porous Surface engineered Lab (SLIPS-LAB) for urinary stone diagnostics

The SLIPS-LAB was designed as a point-of-care (POC) device that facilitates urinary stone diagnostics (**Figure 2-1a**). The SLIPS-LAB allowed patients to test urine samples directly after collection, achieved the tests with minimized manual procedures, and evaluated the urinary stone related metabolic workups (e.g., calcium, uric acid, citrate, oxalate, and pH) within 30 min. To carry out the tests, the SLIPS-LAB was capable of

performing sampling, zero-powered sample loading, and detection in a POC setting (**Figure 2-1b**). The sampling was implemented using the loading leg of the SLIPS-LAB, which was engineered to draw the liquid sample (e.g., urine) by fetching the loading leg in the liquid. Zero-powered loading was designed on the SLIPS-LAB to transport the sample from the loading leg to the designated location. This zero-powered loading was attributed to the structure of the SLIPS-LAB that provides driven force to automate this process [34-43] and the nature of the SLIPS material that significantly reduces the contact angle hysteresis and the friction on the sample-substrate interface [33, 44-50]. Moreover, there was hardly loss of the analyte in the loading process due to the rarely bonding between chemicals and the SLIPS material [51-56]. Finally. the analyte was detected in the reaction chamber where the sample met with required reagents to perform biochemical assays. In particular, the urinary stone related metabolic workups were examined using colorimetric assays and the readout was accomplished using a scanner.

The feasibility of managing viscous fluids and biological fluids has been demonstrated on the SLIPS-LAB (**Figure 2-1c, Supplementary Figure S2-1, and Supplementary Movie S2-1**). Both types of the fluids were loaded in the loading legs (**Figure 2-1c, t= 0 s**). The viscous fluids included water, milk, juice, glycerol, syrup, and honey with viscosity ranging from 1 to ~ 5000 cP in an ascending order (**Supplementary Table S2-1**). These fluids might be of interest for environmental monitoring, food industry, quality control, and so on. The biological fluids contained urine, saliva, tracheal aspirate (TA), plasma, human whole blood, and water, which covered the major domain of samples for diagnostics. The zero-powered sample loading was initialized when the air channel

was unsealed and a net driven force was generated on the samples. All the samples were loaded from the loading legs towards the reaction chambers (**Figure 2-1c, t= 0-6 s**). The loading speed was inversely related to the viscosity of the sample and could lead to significantly different loading time among samples (**Supplementary Figure S2-1 and Supplementary Movie S2-1**). The samples were automatically mixed in the chambers subsequently (**Figure 2-1c, t= 670/ 92 s**). To note, there was no visible residual sample stained on the channels after the loading in all cases.

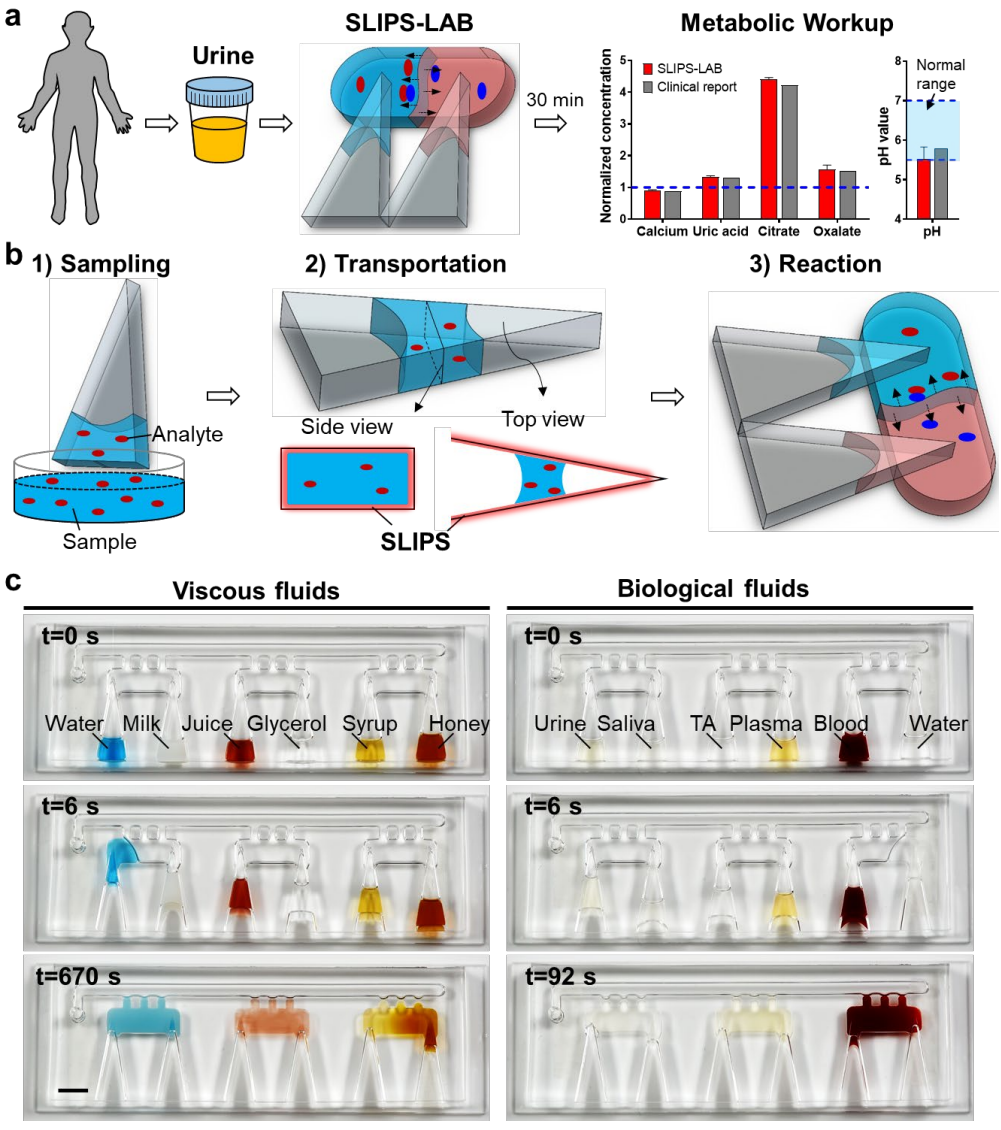

Figure 2-1. Slippery Liquid-Infused Porous Surface engineered Lab (SLIPS-LAB) for point-of-care diagnostics. (**a**) Overview of urinary stone diagnostics using SLIPS-LAB. Diagnostics was demonstrated using the SLIPS-LAB in a clinical study and compared with the clinical report. (**b**) The SLIPS-LAB achieves sampling, zero-power loading, and detection processes in a point-of-care manner. Analyte can be sampled, transported on the SLIPS material, and detected using colorimetric assays. (**c**) The SLIPS-LAB is capable of managing various of viscous fluids and biological fluids. Images are representative for at least two independent experiments. Scale bar, 5 mm.

2.2.2 Design of the SLIPS-LAB

The SLIPS-LAB was designed to perform accurate sampling, zero-powered loading, tunable loading time, and mixing for detection (**Figure 2-2a and Supplementary Movie S2-2**). To functionalize this design, the SLIPS-LAB was fabricated using soft lithography and surface coating technique (**Supplementary Figure S2-2**). In brief, a 3D mold was created by bonding two layers of laser machined acrylic sheets. Polydimethylsiloxane (PDMS) was poured on the mold and peeled off to replicate the mold after curing. This PDMS layer was bonded with a PDMS sheet to form the device. The device was lubricated with hydroxylated PDMS, which would bond with the solidified porous PDMS and fixed *in situ* to generate SLIPS on the surface (**Supplementary Figure S2-2b**) [53, 57].

We studied two mechanisms to accurately sample liquid samples in a large volume range (**Figure 2-2a, step 1**). To sample liquid in small volumes, surface tension was able

to hold the liquid in an engineered hole when a droplet passed through the hole (**Figure 2-2b**). The sample volume ranged from 1 μL to 15 μL depending upon the dimensions of the hole, including the diameter and the height (**Figure 2-2g, Supplementary Figure S2-3, and Supplementary Movie S2-3**). To sample liquid in large volumes, hydrostatic force and surface tension served as the leading forces to draw liquid from a container when the other end of the loading channel was sealed (**Figure 2-2c, Supplementary Figure S2-4a, and Supplementary Discussion 2-1**). Briefly, the surface tension was the dominating force in small channels while hydrostatic force was the dominating force in large channels. According to the analysis, the height of the liquid (i.e., water in this calculation) could be taken from the substrate was more than 0.14 m. It met our experimental requirements where the sample were typically less than 5 mm. The sample volume was investigated with the height of the substrate liquid and the dimensions of the loading channel (**Figure 2-2h and Supplementary Figure S2-4b-d**). Complemented to the sampling for liquid in small volumes, this mechanism allowed to sample liquid lying in 10 μL to 50 μL. The sample volume was not sensitive to the converging angle of the loading channels (**Supplementary Figure S2-5**).

Zero-powered sample loading was achieved on the SLIPS-LAB (**Figure 2-2a, step 2-3**). The mechanism of this process was studied in the physical model and the experimental observations (**Figure 2-2d, Supplementary Figure S2-6, and Supplementary Discussion 2-2**). In the physical model, the leading force was the net force between the Laplace pressure on the two air-liquid interfaces and the surface tension on the interfaces. The net force was simplified to an equation with one variable using two

assumptions, including negligible gravity and small contact angle hysteresis. The variable could be the converging angle of the loading leg, the dimension of the sample, or other parameter of interest; while the other parameters were projected in the format of this variable. The physical model uncovered that the loading speed was positively correlated with the converging angle and the thickness of the loading channel. Experimental results suggested same trend (**Figure 2-2i, Supplementary Figure S2-6b, and Supplementary Movie S2-4**). The sample remained static in the channel with no converging angle throughout the experiment. The loading time was tuned between 3 s to 241 s by engineering the converging angle between 5° and 20° and the thickness of the loading channel between 0.75 mm to 3.0 mm. Owing to this mechanism, tunable loading time was accomplished for samples transported through properly designed channels (**Figure 2-2a, step 3**). In this experiment, the converging angle was 20° on the left loading leg and 5° on the right one and the thickness of the device was 3.0 mm. The feasibility of this design was further demonstrated using human whole blood sample on an identical device (**Supplementary Movie S2-5**). The results suggested the same trend with water. To note, there was no blood residual on the loading channels after the loading process.

A 3D channel structure was developed to lead the sample from the loading channel to the reaction chamber for mixing and detection (**Figure 2-2a, step 4**). The 3D channel design was able to resort to the dominating force between the Laplace pressure and the surface tension to complete the transition (**Figure 2-2e and Supplementary Figure S2-7**). The Laplace pressure served as the dominating force to drive the sample until the interface between the loading channel and the reaction chamber. Taking advantage of the

3D channel design, the sample was advanced to the end of the top layer, which was beyond the interface on the bottom layer (**Supplementary Figure S2-7a, step 1 and Figure S2-7b, step 4**). This location mismatch could drive the sample to touch the bottom layer. The surface tension was subsequently dominating to spread the sample into the reaction chamber due to the significantly increased air-liquid interface on the leading edge (**Supplementary Figure S2-7a, step 2-3 and Figure S2-7b, step 5-6**). The mixing happened as the samples contacted. For instance, the sample in the loading hole was first mixed with the sample loaded from the left leg (**Figure 2-2a, t= 10-28 s and Figure 2-2f, step 1**). The sample from the right loading leg could contact the mixture on the left portion, overcome the oil obstacle in between, and mix with the mixture automatically (**Figure 2-2a, t= 36-153 s and Figure 2-2f, step 2-4**). The reusability of the SLIPS-LAB was demonstrated as well (**Supplementary Figure S2-8**).

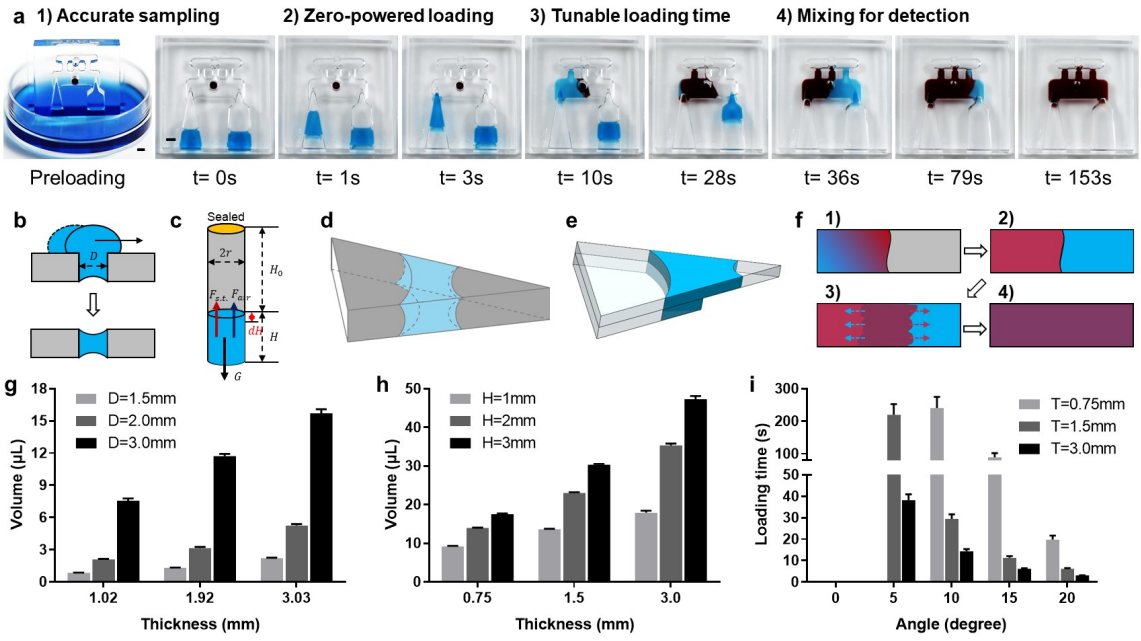

Figure 2-2. Design of the SLIPS-LAB. (**a**) The SLIPS-LAB can implement accurate sampling, zero-powered loading, tunable loading time, and mixing in one device. Images are representative for two independent experiments. Scale bar, 2 mm. (**b-c**) Mechanism of sampling liquid at the large and small volume, respectively. (**d**) Mechanism of the zero-powered loading process. The feasibility of tuning loading time can be demonstrated. (**e-f**) Mechanism of leading the samples into the reaction chamber and the mixing process. (**g-h**) Quantitative analysis of the sampling for large and small volume range, respectively. The data represent mean ± SEM. Each data point was collected from 10-30 independent tests. (**i**) Quantitative analysis of tuning the loading time using different designs. The data represent mean ± SEM. Each data point was collected from 10-20 independent tests.

Chapter 3

Detection of stone related metabolic workups on the SLIPS-LAB

In this chapter, we will describe the design of the SLIPS-LAB for multiplex detections and the respective fabrication process. The feasibility of detecting urinary stone related metabolic workups on the SLIPS-LAB will be proved by the ability of properly performing the corresponding biochemical assays on the SLIPS-LAB and the calibration of examining the target concentration using these colorimetric assays. Pre-clinical study of testing target metabolic workups in a volunteer's urine sample will be demonstrated to verify the coordination between the SLIPS-LAB and the standard methods. There results will collectively serve as the fundamentals of performing further clinical studies using the SLIPS-LAB.

3.1 Materials and methods

In this section, we will explain the design of the SLIPS-LAB to enable multiplex detections and descript the fabrication process. The design of performing the biochemical assays of detecting urinary stone related metabolic workups on the SLIPS-LAB will be investigated. The protocols of performing these biochemical assays and corresponding calibration process (e.g., data analysis) will be studied. The procedures of performing the test for a volunteer's urine sample will be discussed.

3.1.1 Design of the SLIPS-LAB for multiplex detection

The SLIPS-LAB consisted of six units for performing multiplex detections where each unit was designed with two loading legs and a reaction chamber. There were holes punched on top of the reaction chambers to sample liquid in small volume. The inner diameter of the punch was 1.5 mm and 2.0 mm. The height of the holes was 2.0 mm and 3.0 mm. The holes were localized either in the center of the reaction chambers or near one loading leg. The converging angle of the loading legs was 5° and 20°. The thickness of the loading legs was 1.5 mm and 3.0 mm, which tuned the volume of the samples. Multiple liquid samples were loaded from a microwell array to the loading legs following the sampling protocols mentioned above. The microwell array was fabricated by bonding a laser machined acrylic sheet at the thickness of 3 mm with a glass slide. The diameter of the microwell was 10 mm. The liquid volume was 190 μL in each microwell in the loading process. The integration of these designs functionalized the SLIPS-LAB to carry out individual assay in each unit.

3.1.2 Characterization of detecting urinary stone-related metabolic workups

Commercial assay kits were calibrated and applied to determine the metabolic workup in urine in the clinical studies. The calcium assay kit was from Cayman (701220). The uric acid assay kit was from BioAssay Systems (DIUA-250) and the uric acid was bought to calibrate this assay kit (Sigma, U2625-25G). In the calibration, the uric acid was dissolved in 0.1M Tris-HCl (pH=7.2). The citrate and oxalate assay kits were from Sigma (MAK057 and MAK179, respectively). The pH indicator was from MsLavenda.com. The

pH buffer, ranging from 5.06 to 7.61, was prepared by mixing citrate acid (0.1 M) and disodium phosphate (0.2 M) following the reference protocols (**Supplementary Table S3-1**) [58]. The TM buffer (1x) was applied as the buffer with pH value at 8.21.

The characterization was achieved using standard methods following manufacturer's instructions. The instructions are available online. The readout was achieved using FlexStation 3, Molecular Devices. To note, the pH parameter was not calibrated using the standard method from the manufacturer and was detected using a pH meter (HI 2210, HANNA instruments) or pH strips (Multistix 10 SG, SIEMENS) in the clinical studies. The characterization was also performed using the SLIPS-LAB. The design of the SLIPS-LAB was detailed above. First, the target samples were loaded into the holes locating on top of the reaction chambers when the tissue paper passed through the holes. The target samples were the samples containing corresponding ions at different concentrations for the calcium, uric acid, and citrate assays; whereas the target samples were the chemicals used to test the ions for the oxalate and pH assays. Secondly, the loading legs were dipped in the microwells, where reagents were pre-loaded and the volume was 190 μL. The reagents were detailed in each assay. Thirdly, the reagents were sampled from the microwells and the zero-power loading was achieved as described above. Fourthly, the assays were manually mixed by shaking the device left and right for 5 min and incubated for 10 min at room temperature in dark. Finally, the colorimetric assays were tested using a scanner (MX860, Canon). The RGB elements were obtained at the middle of the loading hole and one loading leg in each assay. To reduce the testing error, each assay was triple scanned and a region of 11 × 11 pixel was selected to evaluate the

RGB elements. The most sensitive color element was selected to build up the calibration curve for each assay. The linear curve fitting was performed for each calibration curve in GraphPad Prism software.

3.1.3 Pre-clinical study of detecting urine from a volunteer

Spot urine was collected from a healthy volunteer and stored at 4 degree Celsius (collected at 9:00 am on 04/06/18, ~40 mL in total). The metabolic workups were tested using the standard methods and the SLIPS-LAB in parallel. The results were determined using the calibration curves in both methods.

3.2 Results and discussions

In this section, we will present the detailed engineering design of the SLIPS-LAB for multiplex detections. The capability of performing colorimetric assays for detecting urinary stone related metabolic workups using the SLIPS-LAB will be demonstrated. The characterization of these colorimetric assays will be investigated. The translational potential will be validated by the high coordination between the SLIPS-LAB and the standard methods for examining a volunteer's urine sample.

3.2.1 Design of the SLIPS-LAB for multiplex detection

The SLIPS-LAB was designed to conduct multiplex detection in parallel (**Figure 3-1a-d, Supplementary Figure S3-1a-b, and Supplementary Movie S6**). We

engineered the thickness and the converging angle of the loading legs to sample liquid in large volumes (**Figure 3-1a-b**). In particular, the thickness was 1.5 mm and 3.0 mm and the converging angle was 20° and 5°. These loading legs could sample various of liquid from a laser machined microwell array where the height of the liquid was set to 3 mm. According to the calibration, the sampled volume was 30 μL and 47 μL (i.e., mean value) in the loading legs at the thickness of 1.5 mm and 3.0 mm, respectively (**Figure 2-2h**). The different converging angle was designed to tune the loading time. In the current design, the loading time difference should be around 220 s (**Figure 2-2i**). The diameter, height, and location of the holes, which were on top of the reaction chambers, was investigated to sample liquid in small volumes (**Figure 3-1c and Supplementary Figure S3-1b**). The diameter were set using punch at diameter of 1.5 mm, 2.0 mm, 1.5 mm, 1.5 mm, and 1.5 mm and the height were designed to 3.0 mm, 3.0 mm, 3.0 mm, 2.0 mm, and 2.0 mm from left to right while there was no hole on the end right chamber. Based on the calibration, the volume was 2.2 μL, 5.2 μL, 2.2 μL, 1.4 μL, and 1.4 μL (i.e., mean value) in the holes from left to right correspondingly (**Figure 2-2g**). The feasibility of performing multiplex detections was demonstrated using the SLIPS-LAB. The sampling process was achieved following the procedure mentioned above (**Supplementary Figure S3-1a, 1st part and Supplementary Movie S2**). The zero-powered loading was launched when the air channel was unsealed. The samples moved faster in the left six channels that were at larger thickness than the right ones. The samples from the loading legs and the small holes mixed together as they contacted. Owing to the converging angle difference, the sample in the eighth loading leg was first loaded and mixed with the sample from the small hole, which was significantly faster than the left neighbor sample. Manual mixing was conducted to

speed up the mixing process. The RGB color elements of the samples would be subsequently determined using a commercialized scanner.

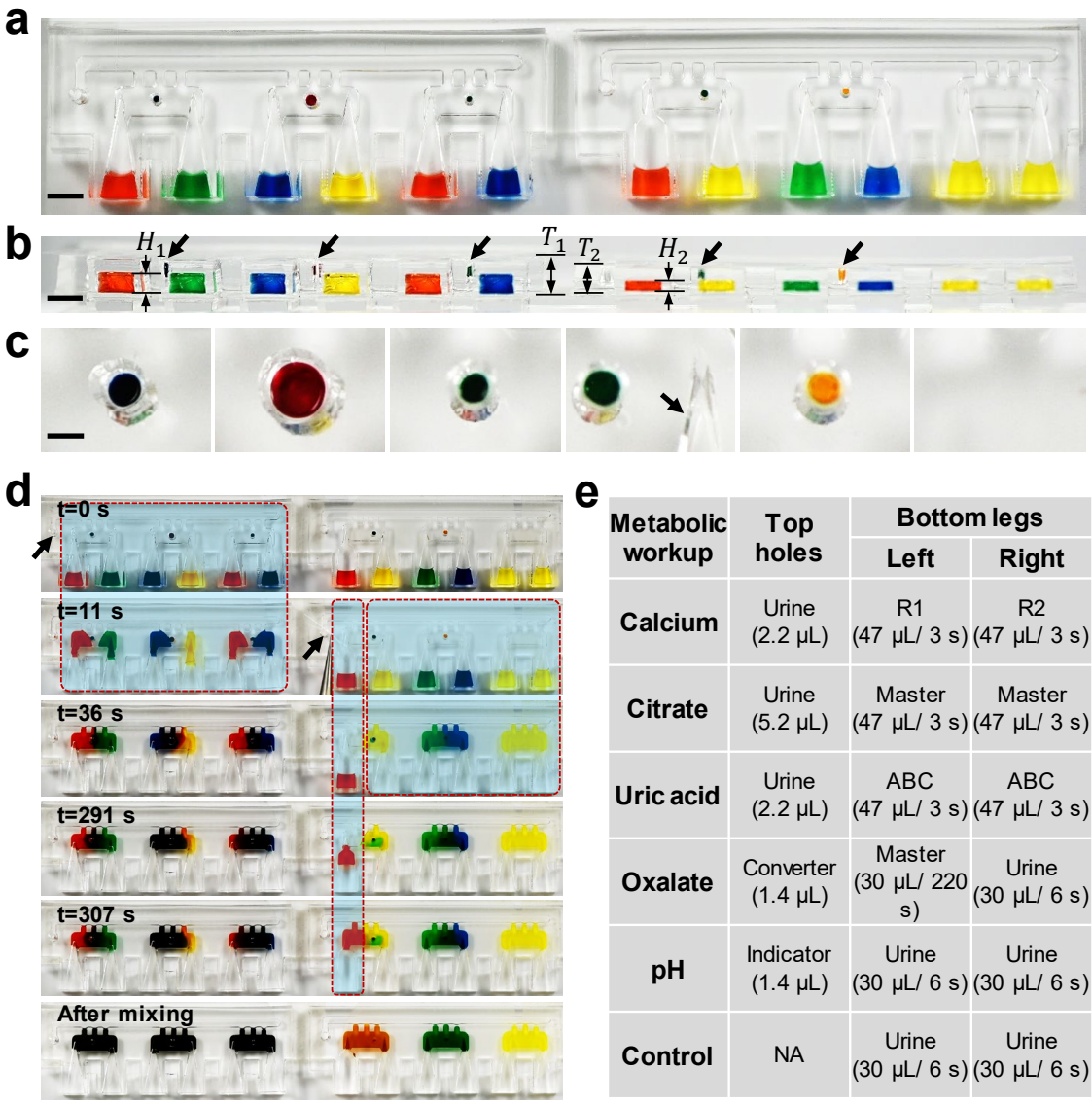

e

Metabolic workup	Top holes	Bottom legs	
		Left	Right
Calcium	Urine (2.2 μL)	R1 (47 μL/ 3 s)	R2 (47 μL/ 3 s)
Citrate	Urine (5.2 μL)	Master (47 μL/ 3 s)	Master (47 μL/ 3 s)
Uric acid	Urine (2.2 μL)	ABC (47 μL/ 3 s)	ABC (47 μL/ 3 s)
Oxalate	Converter (1.4 μL)	Master (30 μL/ 220 s)	Urine (30 μL/ 6 s)
pH	Indicator (1.4 μL)	Urine (30 μL/ 6 s)	Urine (30 μL/ 6 s)
Control	NA	Urine (30 μL/ 6 s)	Urine (30 μL/ 6 s)

Figure 3-1. SLIPS-LAB for multiplex detection. (**a-c**) The engineering design of the SLIPS-LAB for multiplex detection. Scale bar, (a) and (b), 5 mm; (c) 1 mm. (**d**) Demonstration for multiplex detections, including sample loading, time control, and mixing for detection. Images are representative for two independent experiments. (**e**) The

design of SLIPS-LAB to perform the colorimetric assays to test the urinary stone related metabolic workups.

3.2.2 Colorimetric detection of urinary stone related metabolic workups on the SLIPS-LAB

Colorimetric detections were implemented to test the most significant urinary stone related metabolic workups using the SLIPS-LAB, including the calcium, citrate, uric acid, oxalate, and pH value (**Figure 3-1e-f**). The chemical assays were designed on the SLIPS-LAB following the mechanisms from manufacturer's instructions (**Supplementary Table S3-2**) [59]. Minor modifications were applied to fit the physical design of the SLIPS-LAB. For instance, the chemical reactions were identical with the initial design but the ratio between the chemicals and the sample to test might vary with the instructions. The details were explained for each assay, including the reagents to be sampled, the volume of each reagent, and the estimated reaction time of each reagent (**Figure 3-1e and Supplementary Figure S3-1c**). The chemical assays were calibrated on the SLIPS-LAB. Briefly, the chemical reactions were launched following the procedures of sampling, zero-powered loading, and mixing. The assays were examined using a scanner and the RGB color elements were analyzed in Adobe Photoshop. The concentrations of the metabolic ions were studied with the change of the RGB color elements and represented with the most sensitive color element or the combination of the sensitive color elements (**Figure 3-2a and Supplementary Figure S3-2**). The calcium, uric acid, and citrate assays were represented by the green element and the oxalate assay was represented by the blue element.

The linear curve fitting was performed to determine the equation of each curve. The pH value was determined by the combination of the red element and the green element, in which the red element was more sensitive than the green element. The equations to determine the pH value were calculated in separated regions.

To demonstrate the feasibility of urinary stone diagnostics on the SLIPS-LAB, preclinical study was conducted for urine sample from a volunteer. The urine sample was tested using the standard methods and the SLIPS-LAB in parallel. The standard methods to test the concentration of calcium, citrate, uric acid, and oxalate in the urine sample were following the instructions of the assay kits, where calibration curves were built up for each assay kit to calculate the concentration of corresponding target (**Supplementary Figure S3-3**). The pH values were tested using pH stripes (**Supplementary Figure S3-4**). The colorimetric assays were performed on the SLIPS-LAB following the protocols mentioned above and the parameters were calculated according to the established calibration curves (**Figure 3-2a and Supplementary Figure S3-5**). The results suggested high coordination between the SLIPS-LAB and the standard methods (**Figure 3-2b and Supplementary Table S3-3**).

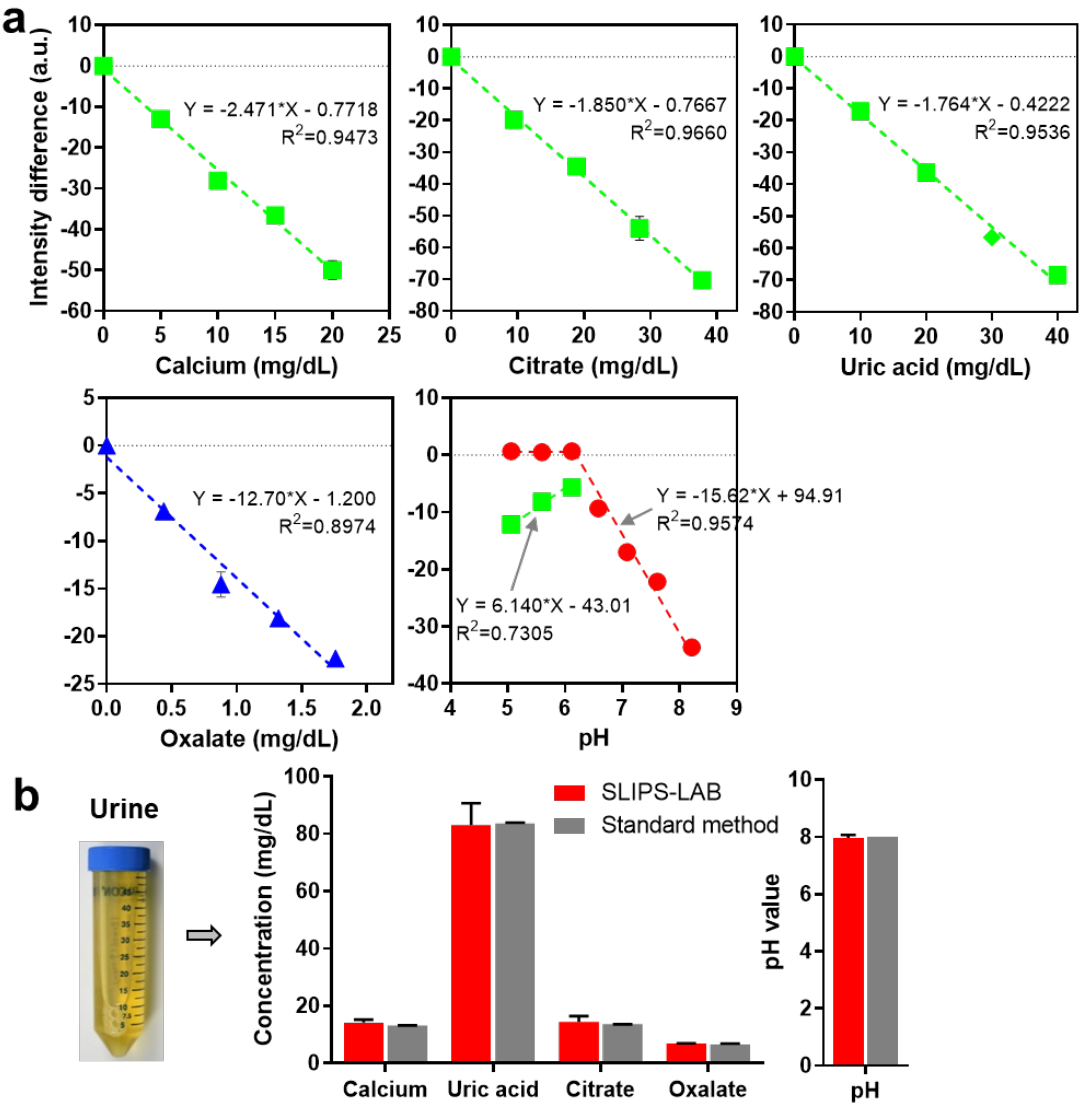

Figure 3-2. Demonstration of kidney stone diagnostics using the SLIPS-LAB. (**a**) Calibration of the colorimetric assays for respective metabolic ions. Different color represents respective color element in the test. The data represent mean ± SEM (n= 3). (**b**) Kidney stone diagnostics on the SLIPS-LAB for a urine sample from a volunteer and the comparison with the results from standard methods. The data represent mean ± SEM (n= 3 using SLIPS-LAB and n= 2 using standard methods).

Chapter 4

Urinary stone diagnostics for clinical samples

In this chapter, we will validate the clinical feasibility of performing urinary stone diagnostics using the SLIPS-LAB for clinical samples directly. In particular, the procedures for collecting urine samples from patients will be described. The procedures of detecting the patients' urine sample will be built up. The results achieved from the SLIPS-LAB will be compared with the clinical reports. Statistical analysis will be conducted to study the coordination between the systems. Finally, the risk of the urinary stone occurrence will be individually estimated for the patients and the personalized treatment will be discussed for patients with distinct stone formation mechanisms.

4.1 Materials and methods

In this section, we will explain the procedures of collecting urine samples from patients and the protocols of performing respective tests on the SLIPS-LAB. The statistical analysis will be introduced for evaluating the results from the SLIPS-LAB that is critical to determine the coordination between the SLIPS-LAB and the clinical reports.

4.1.1 Clinical study of detecting urine directly from patients

Patient urine samples were collected in 24 hours from patients admitted in Veterans Affairs Palo Alto (hospital name), following xx procedures Stanford University Institutional Review Board (IRB) and Veterans Affairs Palo Alto Health Care System (VAPAHCS) Research and Development committee. These patient urine samples were aliquoted into at least three 50 mL plain tubes for parallel tests, two in which were sent to the Quest Diagnostics and The Pennsylvania State University and one was kept in Stanford University (**Supplementary Table S4-1**). The report from Quest Diagnostics served as the gold standard while the others were achieved on SLIPS-LAB using same procedures as determined in the pre-clinical study. Each sample were tested three times.

4.1.2 Statistical analysis

Statistical analysis was performed to find the outliers for the data pair in the clinical study. In brief, there were two criteria to determine the outliers. First, the standardized residual should be larger than 2, which was calculated by residual of the data pair divided by the standard error of the estimate. Second, standardized residual should be inconsistent with its neighbors.

4.2 Results and discussions

In this section, we will perform urinary stone diagnostics using the SLIPS-LAB and evaluate the coordination between the SLIPS-LAB and the clinical reports. In particular,

linear regression analysis will be conducted to study the linearity of the testing results in the detection range. Bland–Altman plot will be applied to better understand the trend, the spot outliers, and the magnitude of disagreement between the systems [60]. The urinary stone occurrence risk will be individually evaluated and the corresponding personalized treatment will be discussed for patients with distinct stone formation mechanisms.

4.2.1 Clinical study of detecting urine directly from patients

We piloted a clinical study to validate the applicability of the SLIPS-LAB for urinary stone diagnostics in clinical settings (**Figure 4-1a**). In this study, the 24 hr urine samples were collected from patients and tested using the SLIPS-LAB and in a central clinical laboratory (i.e., Quest Diagnostics). The raw data obtained from the SLIPS-LAB and the necessary calculation leading to the final results were explained (**Supplementary Table S4-2**). The urinary stone risk was individually evaluated based on the metabolic workups that were normalized with regard to critical concentrations in clinical practices (**Supplementary Table S3-2**). The performance of the SLIPS-LAB was analyzed by comparison with the clinical reports from the central clinical laboratory that served as the gold standard. In particular, linear regression was performed to study the coordination of the SLIPS-LAB with the clinical reports, where the outlier was identified and ruled out in each data set by calculating the residual of the results and the standard error of the estimate in the two detection settings (**Figure 4-1b**). The outliers were highlighted in red and not considered in the analysis. There was one outlier identified in each data set of citrate, uric acid, and oxalate assays, and two outliers in the pH detection. High consistency was

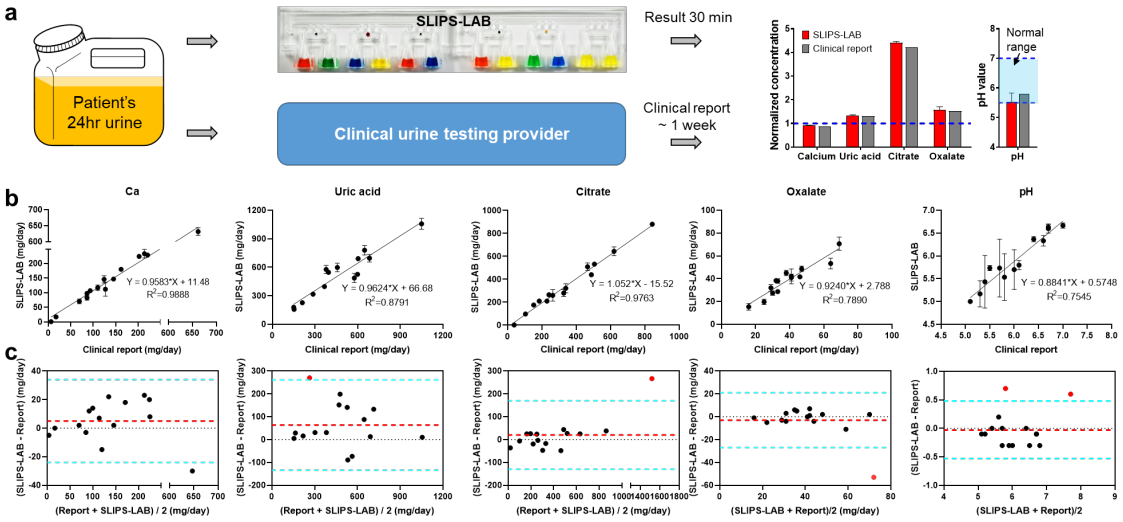

Figure 4-1. Clinical validation of the SLIPS-LAB for kidney stone diagnosis. (**a**) The procedures of performing kidney stone diagnostics using SLIPS-LAB. (**b**) Linear regression of the diagnostic results for each workup from the SLIPS-LAB and the clinical reports. The data represent mean ± SEM (n= 3). (**c**) Bland–Altman plot of the diagnostic results to better assess the trend, the spot outliers, and the magnitude of disagreement between the SLIPS-LAB and the clinical reports.

achieved between the SLIPS-LAB and the clinical reports. For instance, the linear fitting curves for the detections of the calcium and citrate indicated that the slopes of the curves were around 1 and the R-squared values were close to 1. For the uric acid and oxalate detections, the results suggested high coordination between the two detection systems while the residual between the systems became increased in a few data pairs. The pH detections revealed high coordination with the clinical reports as well whereas the SLIPS-LAB had relatively large detection errors in low pH domain that could be attributed to the low resolution in this domain (i.e., pH= 5.0 - 5.5).

To better assess the trend, the spot outliers, and the magnitude of disagreement between the SLIPS-LAB and the clinical reports, the Bland–Altman plot was applied to further evaluate the results (**Figure 4-1c**). The Bland-Altman plot illustrated the distribution of the residual between the two systems (i.e., y-axis) in the detection range (i.e., x-axis). The average of the residual (the red dot line) was presented to explain the overall trend of the error. Compared to the detection range, the offset was negligible for each metabolic workup. Interestingly, the offset of the uric acid detection was enhanced by the several data pairs. The 95% confidence interval (the cyan dot line) was calculated to reveal the spot outliers, which was two times of the standard deviation of the residual. In particular, there was one outlier identified in each detection group (the red dot), four of which were identical with the outliers that were sorted out in the linear regression analysis. The residual distributed randomly over the detection range for each detection group, which indicated that magnitude of the disagreement between the two systems was the random noise that might be resulting from the detection errors, chemical assay errors, and etc.

4.2.2 Personalized treatment for patients at risk of urinary stone

The urinary stone risk was evaluated for each individual according to the metabolic workups and typical cases were collected to show capabilities of the SLIPS-LAB for understanding the mechanism of the stone formation individually and providing insight for personalized treatment. A healthy case was successfully determined using the SLIPS-LAB where all the metabolic workups were in the normal range with low stone occurrence risk, which was compatible with the clinical reports (**Figure 4-2a**). The SLIPS-LAB correctly

identified cases at high risk of stone formation where at least one of the metabolic workups was potentially to lead to problematic solid stone (**Figure 4-2b-d**). For instance, we figured out that patient #6 was at high risk of calcium-oxalate stone which is a very common urinary stone in clinical and typically requires medical treatment for the patient (**Figure 4-2b**). Patient #9 was at high risk of stone due to the low citrate concentration (**Figure 4-2c**). In contrast to the cases at risk of forming one type of stones, patient #15 was potentially to develop both uric acid stone and the calcium-oxalate stone (**Figure 4-2d**). Combination therapy is typically needed to lower the risk and the patient should be followed up more closely.

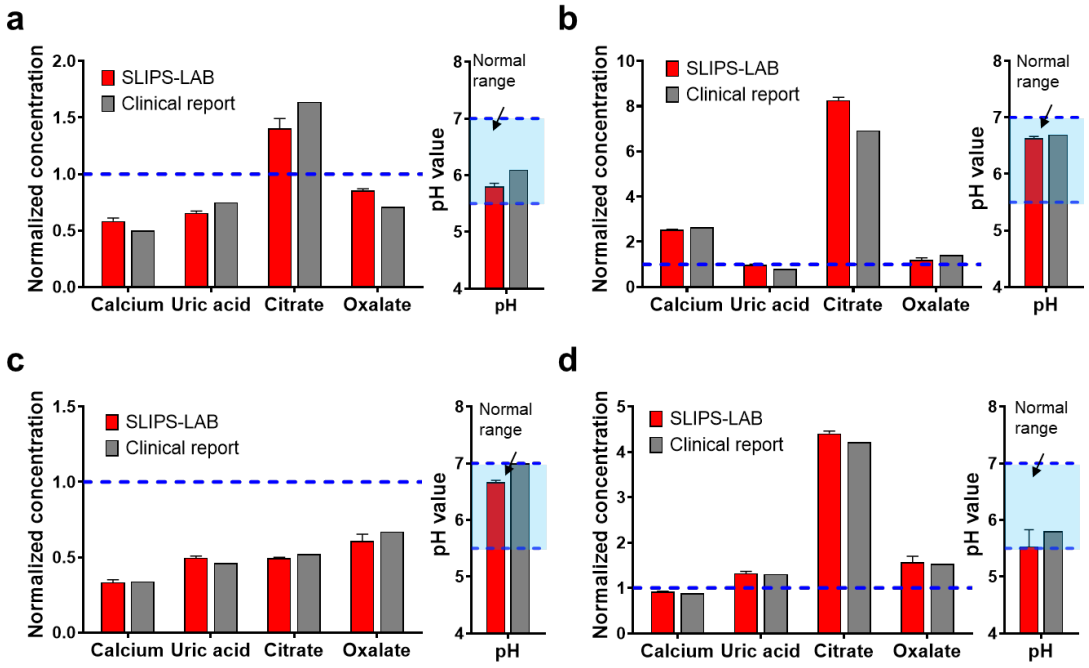

Figure 4-2. Personalized treatment for patients at risk of urinary stone. Urinary stone risk for individuals, including (**a**) the healthy case and (**b-d**) the high-risk cases with distinct stone formation mechanisms.

Chapter 5

Conclusion and future work

In this study, we have developed the SLIPS-LAB for advancing the urinary stone management. The system was designed using the SLIPS material that prevents the target analysts in the sample and significantly reduces friction during the transportation on the interface. The SLIPS-LAB was engineered to automate accurate sampling, zero-powered sample loading, and tunable reaction time control with negligible manual effort. These features have been demonstrated with physical models and experimental setups. The capability of performing multiplex assays was developed on the SLIPS-LAB. The loading legs and the sampling holes were engineered to further functionalize the biochemical assays for detecting urinary stone related metabolic workups. Colorimetric detection assays were achieved on the SLIPS-LAB for detecting calcium, citrate, uric acid, oxalate, and pH, using recommended testing mechanisms. The colorimetric assays were read out using a commercial scanner and the sensitive color elements were employed to study the concentration of respective target metabolic workups. To consolidate the performance of the SLIPS-LAB for clinical study, a pre-clinical study was conducted to detect metabolic workups in a urine sample from a volunteer, where the results suggested high consistency with the standard methods. To validate the clinical feasibility of the SLIPS-LAB for urinary stone diagnostics, we piloted a clinical study for testing 15 urine samples from patients directly. The results indicated high coordination with clinical reports.

Compared with the current guidelines for urinary stone diagnostics, which require high testing cost and long delay in obtaining the results (e.g., the turnaround time is up to 2 weeks), the SLIPS-LAB allows detections in a timely and cost-efficient manner and provides actionable diagnostic information and personalized treatment suggestions to the individuals.

Although the major metabolic workups can be detected using the prototype SLIPS-LAB, we expect to incorporate the diagnostics for the full panel of stone related analysts to strength the capability of predicting the urinary stone risk in the future. This can be promising due to the flexibility and scalability of the SLIPS-LAB. For instance, the SLIPS-LAB can independently and jointly manage the major procedures required to carry out biochemical assays, such as the sampling, the loading, and the reaction steps. One technical consideration lies to the design for assays that require long time intervals between multiple reactions. The maximum time interval is around 5 min in the current design. It can be dramatically elongated to a level of hours frame by manipulating the air channel during the interval of the loading samples. Owing to the design freedom of scaling up assays, the complementary detection panels can be integrated on the SLIPS-LAB with proper engineering designs.

We also expect to further validate the clinical feasibility of the SLIPS-LAB. For instance, it is critical to include a large number of patients to evaluate the performance for predicting the urinary stone risk. Taking advantage of the ability of providing rapid and real-time testing, the SLIPS-LAB might be utilized for monitoring the spot urine on-demand, which may contain of importance information for patients. For example, two

clinical cohorts of high-risk stone formers who will benefit from more intensive monitoring include the uric acid stone formers with acidic urine and the calcium oxalate stone formers with hyperoxaluria. In these scenarios, the SLIPS-LAB represents a significant breakthrough in guiding dietary and pharmacologic treatments for urinary stone formers. Furthermore, it might be potential to overcome the cumbersome collection procedures when the result from a spot urine sample can be representative for the result from the 24-hour urine sample [12, 30].

References

1. Kirkali, Z., et al., *Urinary Stone Disease: Progress, Status, and Needs.* Urology, 2015. **86**(4): p. 651-653.
2. Evan, A.P., et al., *Mechanisms of human kidney stone formation.* Urolithiasis, 2015. **43**(1): p. 19-32.
3. M., G.R., J. Patrick, and S.B. K., *Worldwide Trends of Urinary Stone Disease Treatment Over the Last Two Decades: A Systematic Review.* Journal of Endourology, 2017. **31**(6): p. 547-556.
4. Scales, C.D., et al., *Prevalence of Kidney Stones in the United States.* European Urology, 2012. **62**(1): p. 160-165.
5. Stamatelou, K.K., et al., *Time trends in reported prevalence of kidney stones in the United States: 1976–199411.See Editorial by Goldfarb, p. 1951.* Kidney International, 2003. **63**(5): p. 1817-1823.
6. Romero, V., H. Akpinar, and D.G. Assimos, *Kidney stones: a global picture of prevalence, incidence, and associated risk factors.* Reviews in urology, 2010. **12**(2-3): p. e86-e96.
7. Levin, A., et al., *Global kidney health 2017 and beyond: a roadmap for closing gaps in care, research, and policy.* The Lancet, 2017. **390**(10105): p. 1888-1917.
8. Boyd*, C., et al., *PD12-01- ASSOCIATION OF OBESITY WITH INCREASED ENDOGENOUS OXALATE SYNTHESIS.* 2019. **201**(Supplement 4): p. e220-e221.
9. Lieske, J.C., et al., *Kidney stones are common after bariatric surgery.* Kidney International, 2015. **87**(4): p. 839-845.
10. Uribarri, J., M.S. Oh, and H.J. Carroll, *The First Kidney Stone.* Annals of Internal Medicine, 1989. **111**(12): p. 1006-1009.
11. Cheungpasitporn, W., et al., *Treatment effect, adherence, and safety of high fluid intake for the prevention of incident and recurrent kidney stones: a systematic review and meta-analysis.* Journal of Nephrology, 2016. **29**(2): p. 211-219.
12. Skolarikos, A., et al., *Metabolic Evaluation and Recurrence Prevention for Urinary Stone Patients: EAU Guidelines.* European Urology, 2015. **67**(4): p. 750-763.

13. Tzou, D.T., et al., *Variation in Radiologic and Urologic Computed Tomography Interpretation of Urinary Tract Stone Burden: Results From the Registry for Stones of the Kidney and Ureter.* Urology, 2018. **111**: p. 59-64.
14. Sun, X.-Y., et al., *Size-dependent toxicity and interactions of calcium oxalate dihydrate crystals on Vero renal epithelial cells.* Journal of Materials Chemistry B, 2015. **3**(9): p. 1864-1878.
15. Graham, A., S. Luber, and A.B. Wolfson, *Urolithiasis in the Emergency Department.* Emergency Medicine Clinics of North America, 2011. **29**(3): p. 519-538.
16. Fontenelle, L.F. and T.D. Sarti, *Kidney Stones: Treatment and Prevention.* Am Fam Physician, 2019. **99**(8): p. 490-496.
17. Portis, A.J. and C.P. Sundaram, *Diagnosis and initial management of kidney stones.* Am Fam Physician, 2001. **63**(7): p. 1329-38.
18. Takazawa, R., S. Kitayama, and T. Tsujii, *Appropriate kidney stone size for ureteroscopic lithotripsy: When to switch to a percutaneous approach.* World journal of nephrology, 2015. **4**(1): p. 111-117.
19. Assimos, D., et al., *Surgical Management of Stones: American Urological Association/Endourological Society Guideline, PART I.* Journal of Urology, 2016. **196**(4): p. 1153-1160.
20. Abu-Ghanem, Y., et al., *24-h urine metabolic profile: is it necessary in all kidney stone formers?* International Urology and Nephrology, 2018. **50**(7): p. 1243-1247.
21. Tiselius, H.-G., et al., *Metabolic Work-up of Patients with Urolithiasis: Indications and Diagnostic Algorithm.* European Urology Focus, 2017. **3**(1): p. 62-71.
22. Coe, F.L., A. Evan, and E. Worcester, *Kidney stone disease.* The Journal of Clinical Investigation, 2005. **115**(10): p. 2598-2608.
23. Ludwig, W.W. and B.R. Matlaga, *Urinary Stone Disease: Diagnosis, Medical Therapy, and Surgical Management.* Medical Clinics, 2018. **102**(2): p. 265-277.
24. Dion, M., et al., *CUA guideline on the evaluation and medical management of the kidney stone patient–2016 update.* Canadian Urological Association Journal, 2016. **10**(11-12): p. E348.

25. Ziemba, J.B. and B.R. Matlaga, *Guideline of guidelines: kidney stones.* BJU International, 2015. **116**(2): p. 184-189.

26. Pearle, M.S., et al., *Medical Management of Kidney Stones: AUA Guideline.* Journal of Urology, 2014. **192**(2): p. 316-324.

27. Knoll, T., *Epidemiology, Pathogenesis, and Pathophysiology of Urolithiasis.* European Urology Supplements, 2010. **9**(12): p. 802-806.

28. LOTAN, Y., et al., *Cost-effectiveness of medical management strategies for nephrolithiasis.* Journal of Urology, 2004. **172**(6 Part 1): p. 2275-2281.

29. Ogawa, Y., et al. *Urinary saturation and risk factors for calcium oxalate stone disease based on spot and 24-hour urine specimens*. Frontiers in bioscience : a journal and virtual library, 2003. **8**, a167-76 DOI: 10.2741/1139.

30. Ilich Jasminka, Z., et al., *Comparison of calcium, magnesium, sodium, potassium, zinc, and creatinine concentration in 24-h and spot urine samples in women*, in *Clinical Chemistry and Laboratory Medicine*. 2009. p. 216.

31. Hsi, R.S., et al., *The Role of the 24-Hour Urine Collection in the Prevention of Kidney Stone Recurrence.* Journal of Urology, 2017. **197**(4): p. 1084-1089.

32. Hong, Y.H., et al., *Twenty-four Hour and Spot Urine Metabolic Evaluations: Correlations Versus Agreements.* Urology, 2010. **75**(6): p. 1294-1298.

33. Wong, T.-S., et al., *Bioinspired self-repairing slippery surfaces with pressure-stable omniphobicity.* Nature, 2011. **477**: p. 443.

34. Bai, H., et al., *Efficient Water Collection on Integrative Bioinspired Surfaces with Star-Shaped Wettability Patterns.* Advanced Materials, 2014. **26**(29): p. 5025-5030.

35. Cao, M., et al., *Superhydrophobic "Pump": Continuous and Spontaneous Antigravity Water Delivery.* Advanced Functional Materials, 2015. **25**(26): p. 4114-4119.

36. Chen, H., et al., *Uni-directional liquid spreading control on a bio-inspired surface from the peristome of Nepenthes alata.* Journal of Materials Chemistry A, 2017. **5**(15): p. 6914-6920.

37. Duprat, C., et al., *Wetting of flexible fibre arrays.* Nature, 2012. **482**: p. 510.

38. Heng, X. and C. Luo, *Bioinspired Plate-Based Fog Collectors.* ACS Applied Materials & Interfaces, 2014. **6**(18): p. 16257-16266.

39. Hui Guan, J., et al., *Drop transport and positioning on lubricant-impregnated surfaces.* Soft Matter, 2017. **13**(18): p. 3404-3410.

40. Luo, C., X. Heng, and M. Xiang, *Behavior of a Liquid Drop between Two Nonparallel Plates.* Langmuir, 2014. **30**(28): p. 8373-8380.

41. Ma, X., et al., *Bio-inspired humidity responsive switch for directional water droplet delivery.* Journal of Materials Chemistry A, 2015. **3**(30): p. 15540-15545.

42. Yao, Z. and M.J. Bowick, *Self-propulsion of droplets by spatially-varying surface topography.* Soft Matter, 2012. **8**(4): p. 1142-1145.

43. Zhu, H., Z. Guo, and W. Liu, *Biomimetic water-collecting materials inspired by nature.* Chemical Communications, 2016. **52**(20): p. 3863-3879.

44. Luo, J.T., et al., *Slippery Liquid-Infused Porous Surfaces and Droplet Transportation by Surface Acoustic Waves.* Physical Review Applied, 2017. **7**(1): p. 014017.

45. Dai, X., et al., *Hydrophilic directional slippery rough surfaces for water harvesting.* Science Advances, 2018. **4**(3): p. eaaq0919.

46. Yao, X., et al., *Adaptive fluid-infused porous films with tunable transparency and wettability.* Nature Materials, 2013. **12**: p. 529.

47. Yu, C., et al., *Manipulating Bubbles in Aqueous Environment via a Lubricant-Infused Slippery Surface.* Advanced Functional Materials, 2017. **27**(29): p. 1701605.

48. Dai, X., et al., *Slippery Wenzel State.* ACS Nano, 2015. **9**(9): p. 9260-9267.

49. Wang, J., et al., *Bioinspired Omniphobic Coatings with a Thermal Self-Repair Function on Industrial Materials.* ACS Applied Materials & Interfaces, 2016. **8**(12): p. 8265-8271.

50. Daniel, D., et al., *Oleoplaning droplets on lubricated surfaces.* Nature Physics, 2017. **13**: p. 1020.

51. Yang, S., et al., *Ultrasensitive surface-enhanced Raman scattering detection in common fluids.* PNAS, 2016. **113**(2): p. 268-273.

52. Guan, J.H., et al., *Evaporation of Sessile Droplets on Slippery Liquid-Infused Porous Surfaces (SLIPS).* Langmuir, 2015. **31**(43): p. 11781-11789.

53. Amini, S., et al., *Preventing mussel adhesion using lubricant-infused materials.* Science, 2017. **357**(6352): p. 668-673.

54. Epstein, A.K., et al., *Liquid-infused structured surfaces with exceptional anti-biofouling performance.* PNAS, 2012. **109**(33): p. 13182-13187.

55. Tesler, A.B., et al., *Extremely durable biofouling-resistant metallic surfaces based on electrodeposited nanoporous tungstite films on steel.* Nature Communications, 2015. **6**: p. 8649.

56. Leslie, D.C., et al., *A bioinspired omniphobic surface coating on medical devices prevents thrombosis and biofouling.* Nature Biotechnology, 2014. **32**: p. 1134.

57. MacCallum, N., et al., *Liquid-Infused Silicone As a Biofouling-Free Medical Material.* ACS Biomaterials Science & Engineering, 2015. **1**(1): p. 43-51.

58. Wood, E.J., *Data for biochemical research (third edition)*. Vol. 15. 1987. 97-97.

59. Leslie, S. and K. Bashir, *24-Hour Urine Testing for Nephrolithiasis Interpretation*. 2018.

60. Altman, D.G. and J.M. Bland, *Measurement in Medicine: The Analysis of Method Comparison Studies.* Journal of the Royal Statistical Society. Series D (The Statistician), 1983. **32**(3): p. 307-317.

Appendix A

Supplementary materials for Chapter 2

Supplementary Discussion 2-1

The physical model to sample liquid in a channel was studied as the following figure. The diameter of the channel was $2r$ and the height was $(H_0 + H)$. The liquid was sampled at one end of the channel at the height of H. The other end was sealed prior to drawing the liquid out.

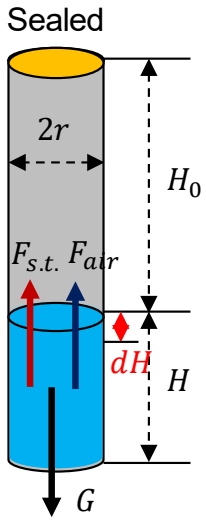

$$\rho\pi r^2 Hg = \Delta P \cdot \pi r^2 + \gamma \cdot 2\pi r \cdot cos\theta \qquad \text{equation 1}$$

$$\Delta P = P_{air} \cdot \frac{dH}{H_0 + dH} \qquad \text{equation 2}$$

Simplified model

r is large: $H - dH = \frac{\Delta P}{\rho g}$ equation 3

r is small: $H = \frac{2\gamma \cdot cos\theta}{\rho g r}$ equation 4

The gravity is the force resisting this motion. There are surface tension and hydrostatic force advancing this motion. At equilibrium stage, the gravity equals to the sum of the advancing force that can be expressed in equation 1-2. In particular, the gravity is calculated by the density and volume of the liquid. The surface tension force is expressed by the surface tension of the liquid and the length of the contacting line on the air-liquid interface. The hydrostatic force is explained by the pressure drop in the top channel due to

the liquid drop (i.e., dH) in this motion and the surface area undergoing this pressure. This model can be simplified to two situations according to the diameter of the channel. The dominating force will be the hydrostatic force when the diameter of the channel is large; while surface tension will be dominating for small channel.

Supplementary Discussion 2-2

Another consideration is the physical model of the zero-powered loading. The channel was designed with a converging angle (i.e., α) and the height of the channel was h. In the calculation, a droplet was located in the channel as shown in the following figure. The dimensions of the droplet (i.e., w, R_1, R_2, $R_1{}'$, and $R_2{}'$) were dynamically related to the location of the droplet (i.e., l_l). The contact angles between the liquid and the solid substrate varied along the radius of the channel (i.e., θ_1 and θ_2).

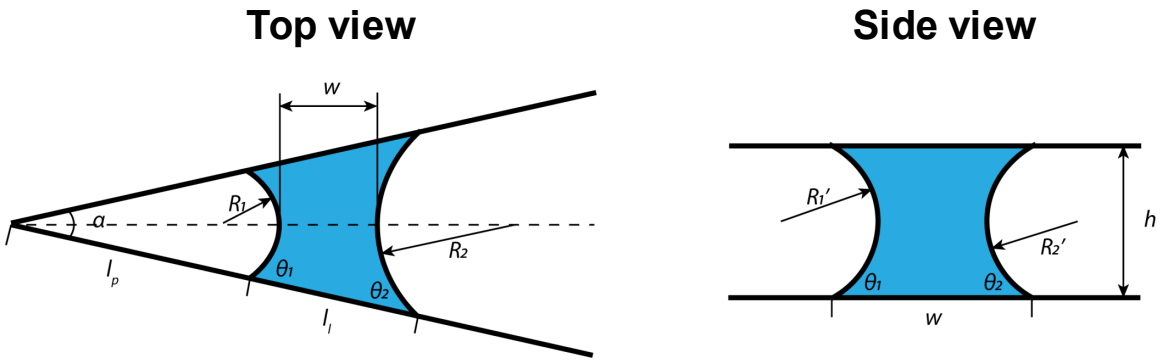

$$F_p = \Delta P_2 A_2 - \Delta P_1 A_1 \qquad \text{equation 5}$$

$$\Delta P_1 = \gamma \left(\frac{1}{R_1} + \frac{1}{R_1{}'}\right) \qquad \text{equation 6}$$

$$\Delta P_2 = \gamma \left(\frac{1}{R_2} + \frac{1}{R_2{}'}\right) \qquad \text{equation 7}$$

$$R_1 = \frac{l_p \sin\frac{\alpha}{2}}{\cos(\theta_1 - \frac{\alpha}{2})} \qquad \text{equation 8}$$

$$R_2 = \frac{(l_p + l_l)\sin\frac{\alpha}{2}}{\cos(\theta_2 + \frac{\alpha}{2})} \qquad \text{equation 9}$$

$$R_1{}' = \frac{h}{2\cos\theta_1} \qquad \text{equation 10}$$

$$R_2{}' = \frac{h}{2\cos\theta_2} \qquad \text{equation 11}$$

$$F_s = 4\gamma\left(l_p + l_l\right) sin\frac{\alpha}{2} cos\,\theta_2 - 2\gamma l_p\, sin\frac{\alpha}{2} cos\,\theta_1 + 4\gamma h\, cos\left(\theta_2 + \frac{\alpha}{2}\right) - 2\gamma h\, cos\left(\theta_1 - \frac{\alpha}{2}\right)$$

equation 12

$$l_l = \sqrt{\frac{2V}{h\,sin\,\alpha} + l_p^2} - l_p \qquad \text{equation 13}$$

$$F_{net} = F_p - F_s \qquad \text{equation 14}$$

There are two types of forces existing on the droplet, including the Laplace pressure and the surface tension. There are two Laplace pressures on the two liquid-air interfaces of the droplet, which can be calculated by the pressure on the surface area (equation 5-7). The dimensions of the droplet can be correlated with the physical design of the channel, the hydrodynamic property of the liquid, and the location of the liquid (equation 8-11). The gravity is negligible to the morphology of the droplet in this calculation. On the other hand, the surface tension also exists on the two liquid-air interfaces that can be presented by the surface tension and the liquid-air contacting lines (equation 12). Because the contact angle hysteresis is significantly reduced to a negligible level using the SLIPS technique (**i.e., < 3° for water**), the model can be simplified by building up the relationship between the location of the liquid and the volume of the liquid (equation 13). The net force is the sum of the Laplace pressure and the surface tension, which can assist to understand the mechanism for the zero-powered loading motion and guide the design of the SLIPS-LAB (equation 14).

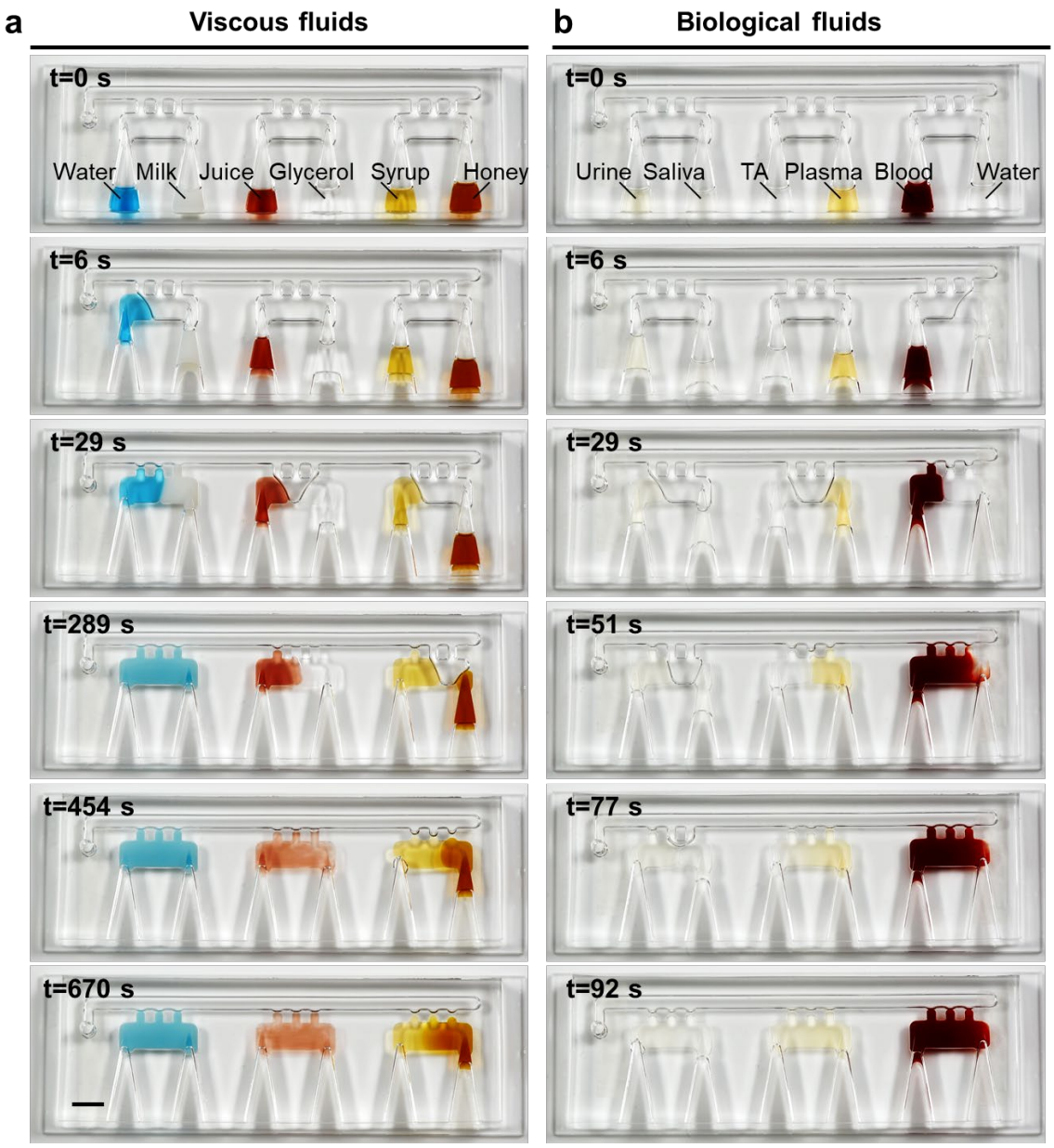

Figure S2-1. SLIPS-LAB for managing various of viscous fluids and biological fluids. (**a**) The details of managing viscous fluids, including water, milk, juice, glycerol, syrup, and honey. (**b**) The details of managing biological fluids, including urine, saliva, trachea sample, plasma, human whole blood, and water.

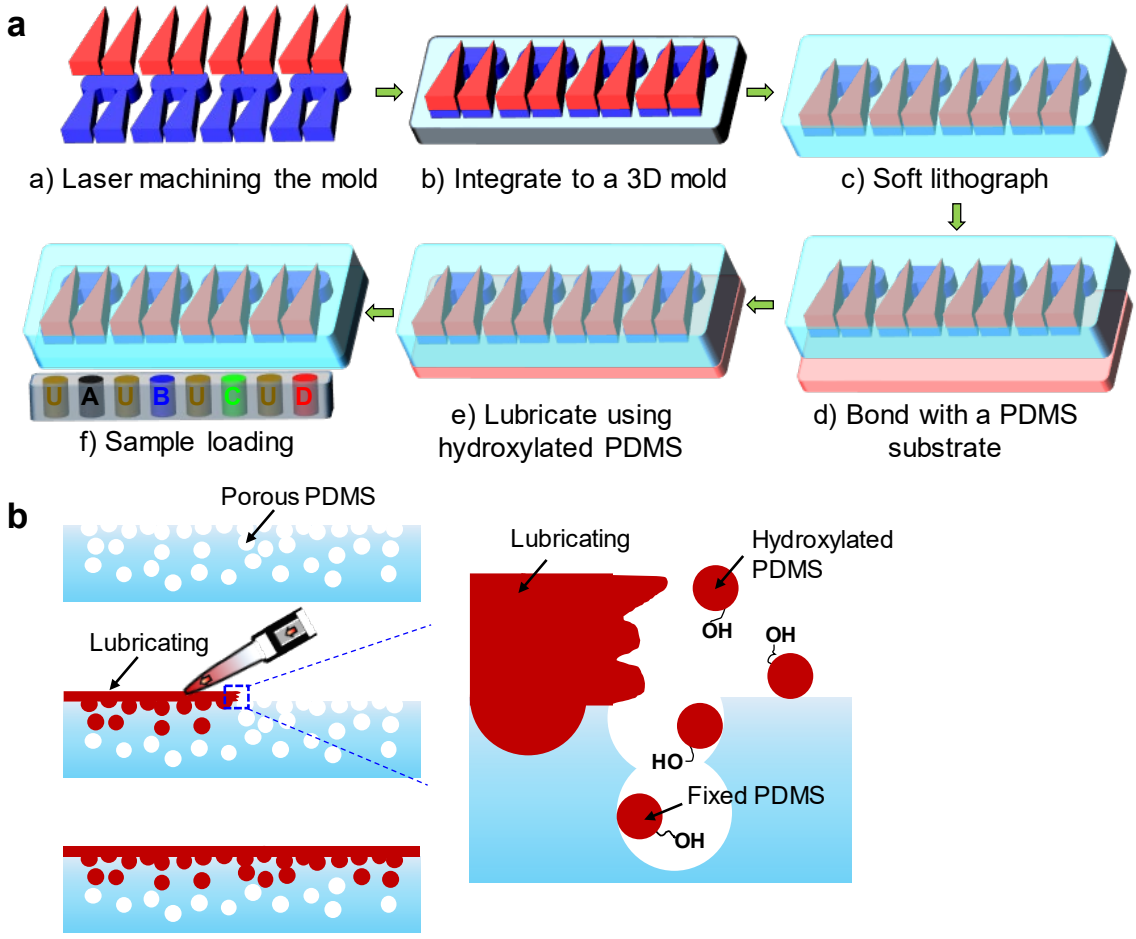

Figure S2-2. Fabrication of the SLIPS-LAB. (**a**) The SLIPS-LAB was fabricated using soft lithography on a laser machined 3D mold. (**b**) The SLIPS was achieved by lubricating hydroxylated PDMS on the device overnight. The hydroxylated PDMS was bonded and locked on the solid PDMS.

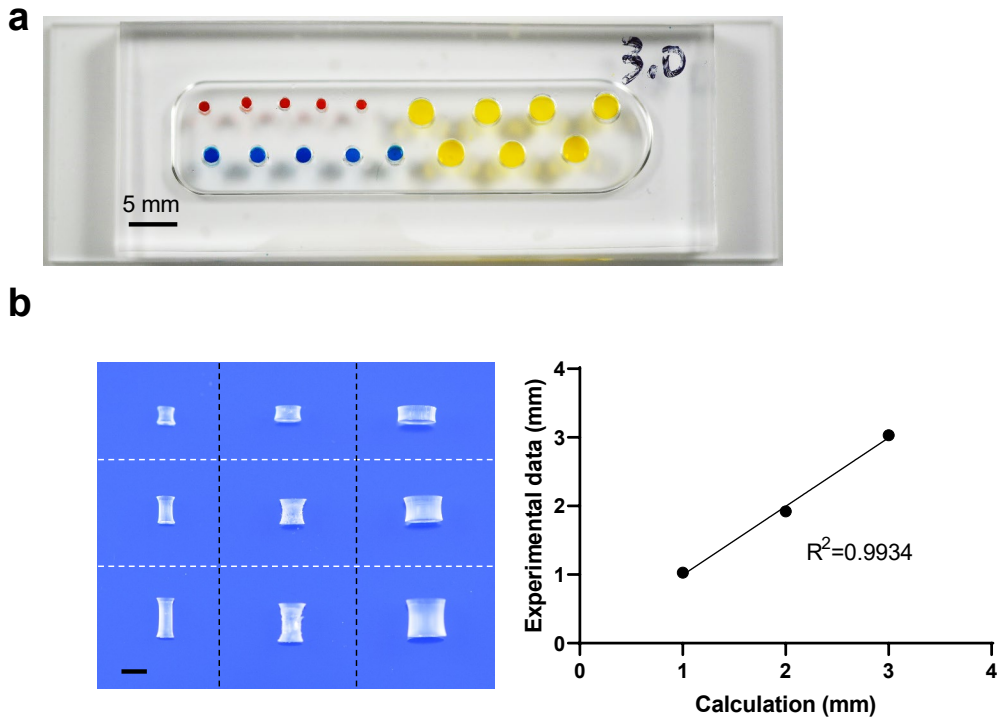

Figure S2-3. Quantitative analysis of sampling liquid in the loading holes. (a) Sampling liquid in the loading holes at the diameter of 1.5 mm, 2.0 mm, and 3.0 mm. The height of the holes was 3.03 mm. (**b**) The profiles of the punched PDMS cylinders with various PDMS thickness (i.e., 1.02 mm, 1.92 mm, and 3.03 mm) and puncher diameter (i.e., 1.5 mm, 2.0 mm, and 3.0 mm). (**c**) The correlation of the PDMS thickness between theoretical calculation and experimental measurements. Each data point represents results from 3 independent devices and each device contains 3 independent PDMS cylinders to be measured. Scale bar, 5 mm and 2 mm in (a) and (b), respectively.

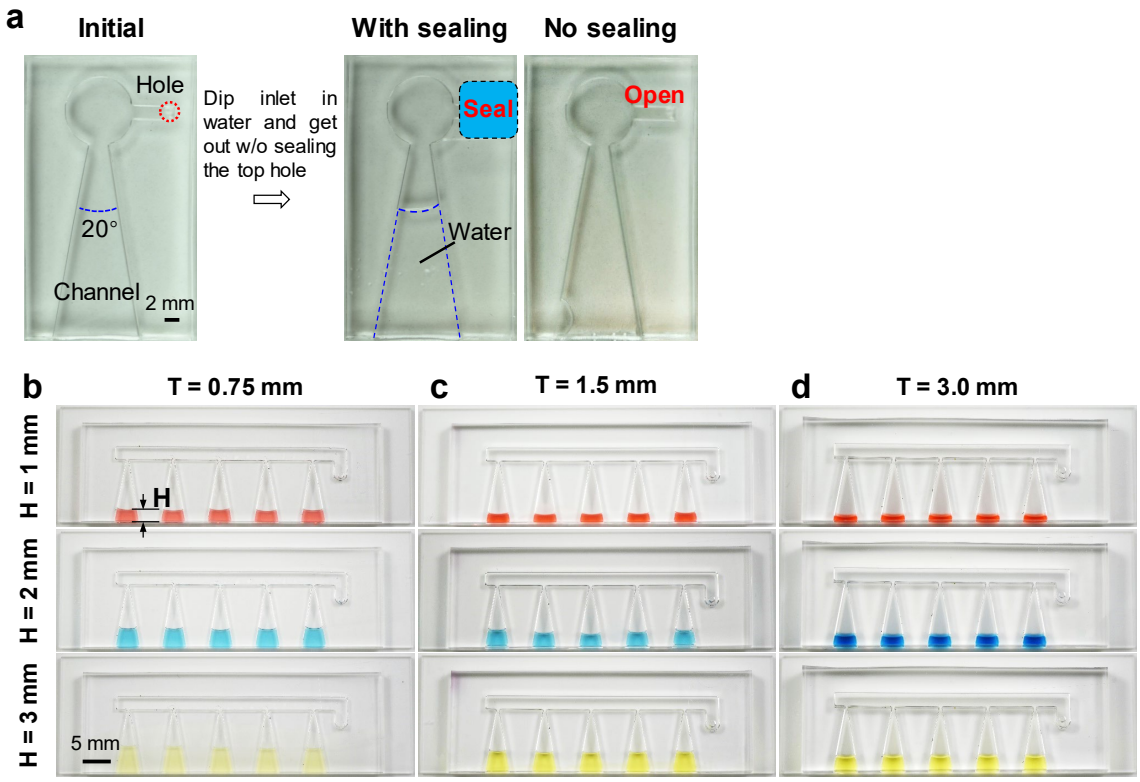

Figure S2-4. Sampling and zero-powered loading using the SLIPS-LAB. (**a**) Demonstration of sampling water on the SLIPS-LAB. (**b-d**) Quantitative analysis of sampling liquid on the loading legs. Sampling liquid at the height of 1 mm, 2 mm, and 3 mm on the loading legs at the thickness of 0.75 mm, 1.5 mm, and 3.0 mm, respectively.

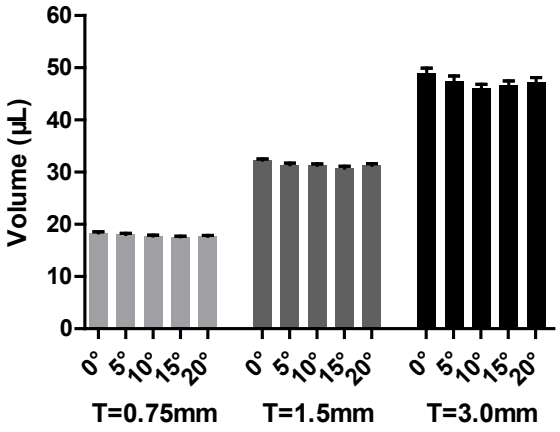

Figure S2-5. Quantitative analysis of sampling liquid with the loading angle. Sampling liquid on the loading legs with converging angle from 0° to 20° with interval of 5°. The thickness of the devices were 0.75 mm, 1.5 mm, and 3.0 mm, respectively. Each data point was collected from 10 independent tests.

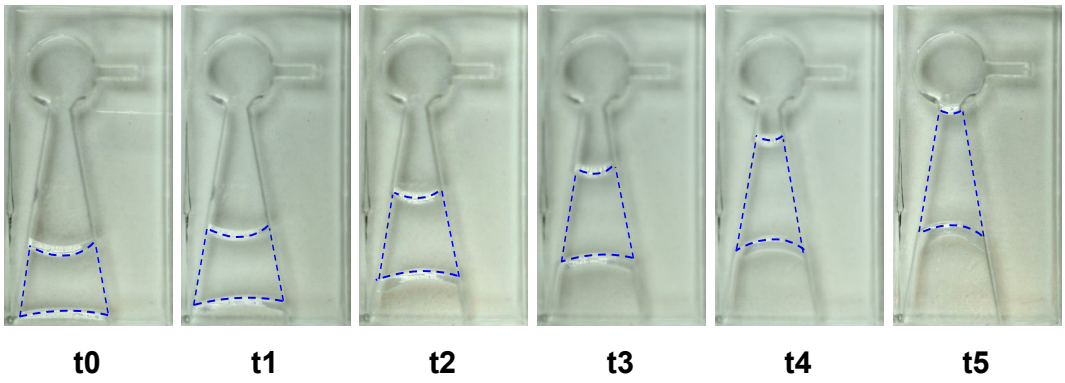

Figure S2-6. Demonstration of the zero-powered loading on the SLIPS-LAB. The sample was loaded from the loading leg towards the chamber over time with no power requirement.

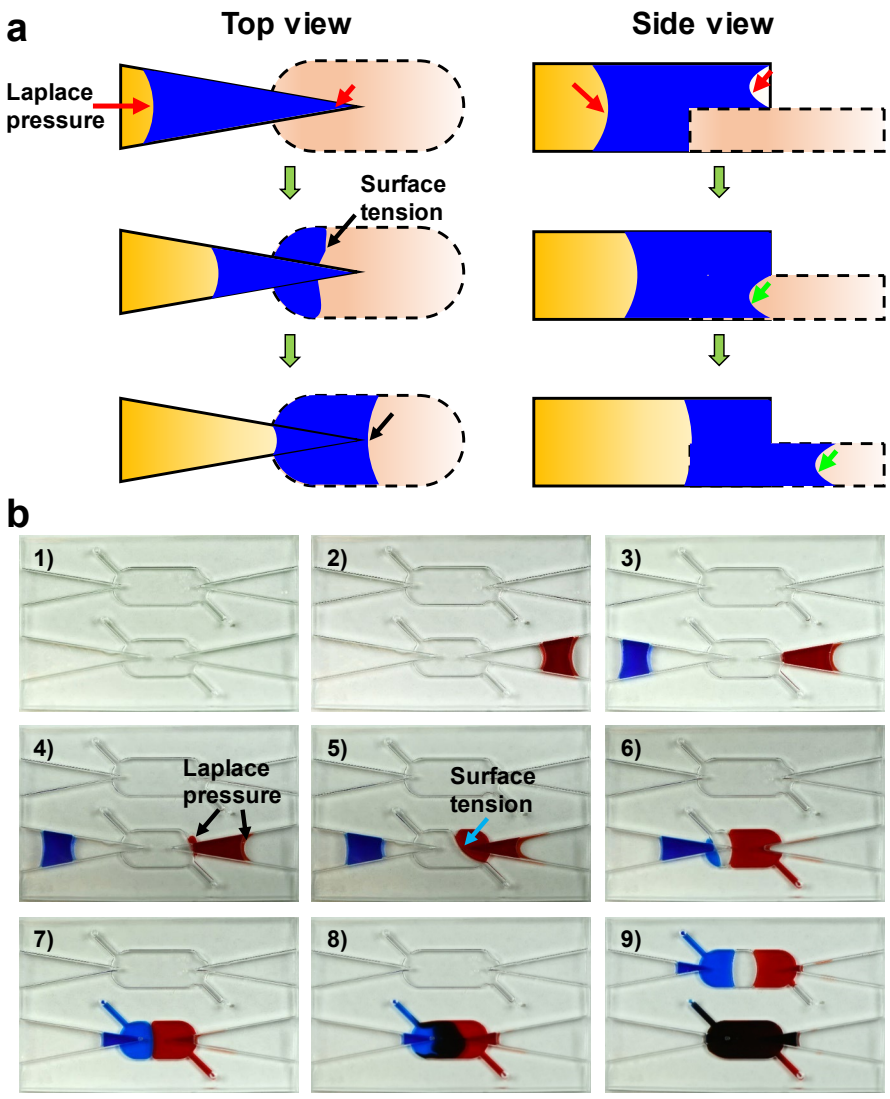

Figure S2-7. 3D channel design leads liquid sample from the channel into the reactor. (**a**) Mechanism of the sample loading at the interface between the loading channel and the reactor. (**b**) Experimental demonstration of the loading at the interface by the Laplace pressure and the surface tension.

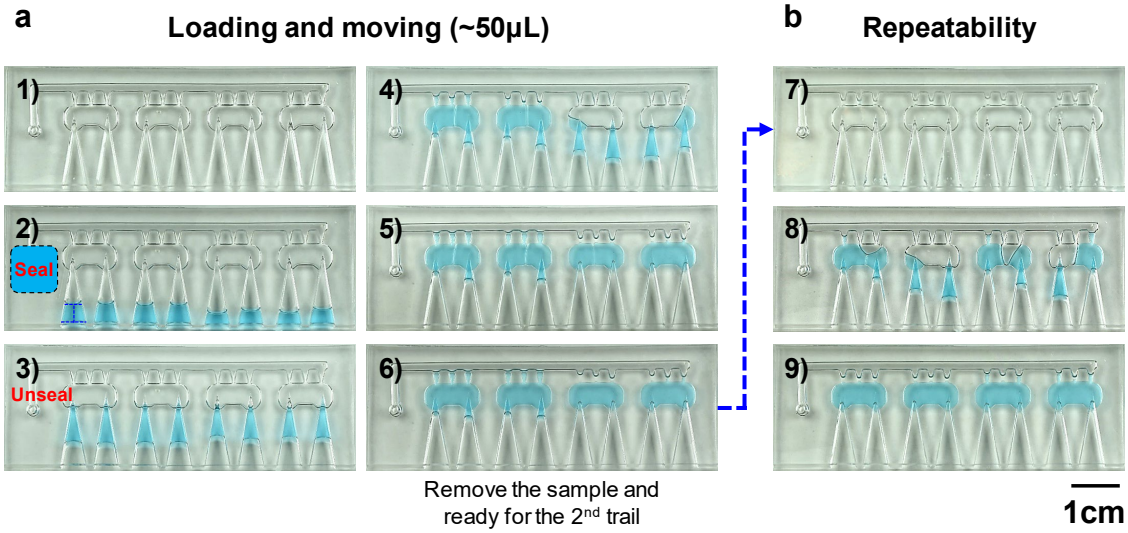

Figure S2-8. Reusability of the device. (**a**) The working details of sampling, loading, and mixing on the SLIPS-LAB. (**b**) The liquid was dumped out from the reactor. The device was reused after cleaning with ethanol for 3 times and re-treating with the hydroxylated PDMS at 55°C for 10 min. Scale bar, 1 cm.

Supplementary Table S2-1. Viscosity of the analytical fluids and the physiological fluids demonstrated on the SLIPS-LAB.

Category	Substance	Viscosity (mPa·s)	Temperature (°C)
Viscous fluid	Water	1	20
	Whole milk	~2	20
	Grape juice	< 20	20
	Glycerol	1412	20
	Syrup, maple	154 - 313	20
	Honey	4500 - 16500	20
Biological fluid	Urine	~1	20
	Saliva	< 5	23
	Tracheal aspirate	38 ~ 32000	20
	Plasma	1.70 ~ 1.92	20
	Whole blood	< 6	20

Appendix B

Supplementary materials for Chapter 3

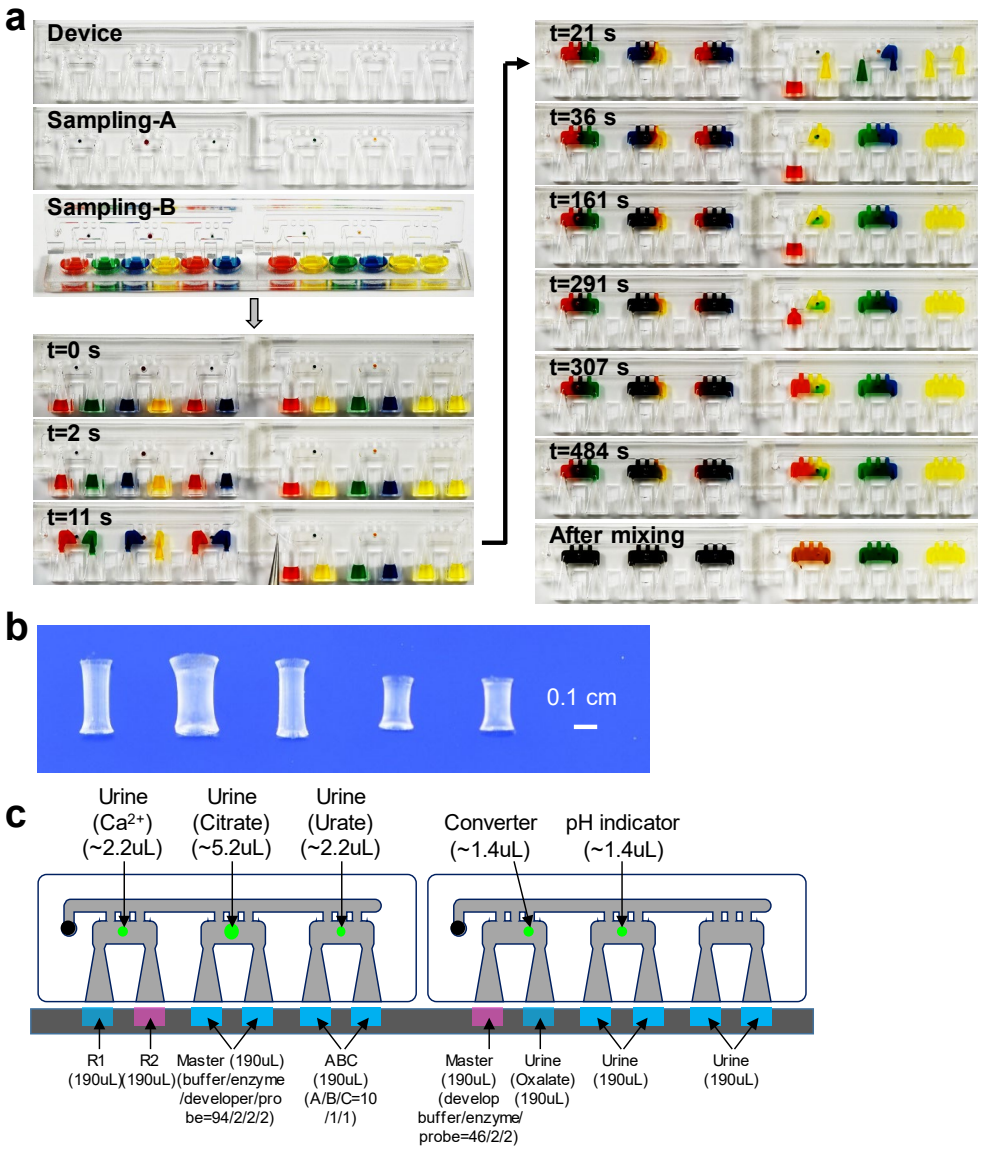

Figure S3-1. The SLIPS-LAB for multiplex detection and the design for the colorimetric assays. (**a**) The details of sampling, zero-powered loading, tuning loading

time, and mixing to achieve the SLIPS-LAB for multiplex detections. (**b**) The profiles of the punched PDMS cylinders from left to right on the SLIPS-LAB to engineer the sampling for liquid in small volumes. Scale bar, 1 mm. (**c**) The design of the colorimetric assays on the SLIPS-LAB. The chemicals, the patterns, and the estimated volume were explained.

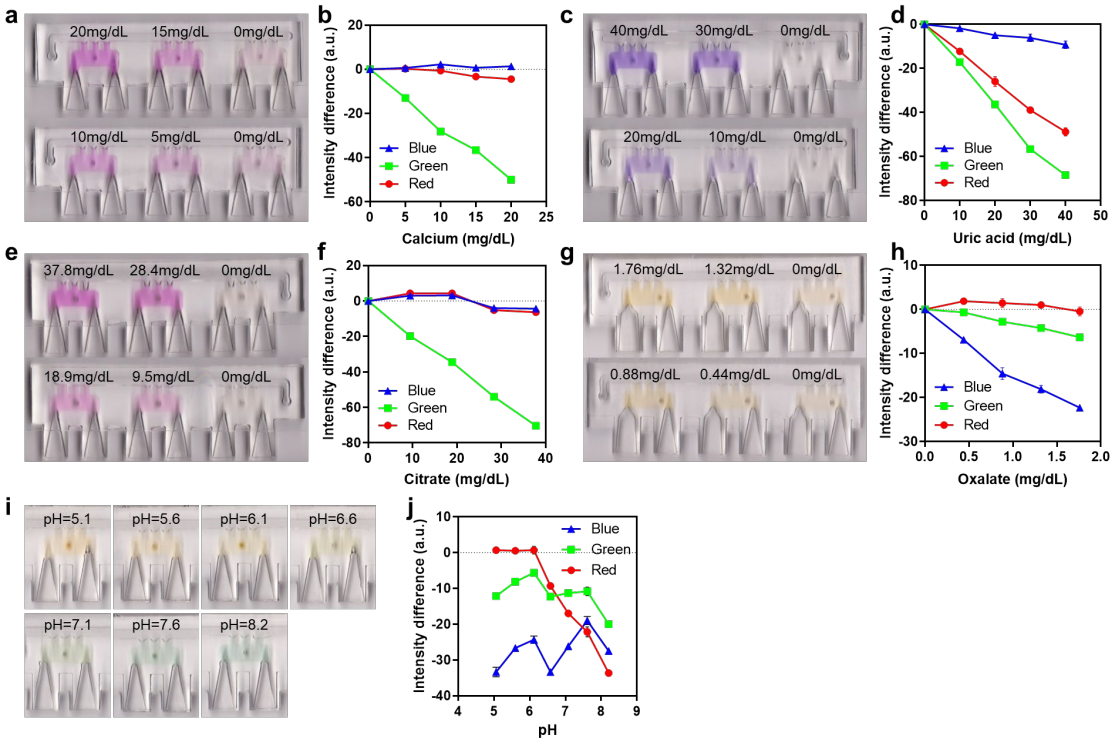

Figure S3-2. Calibration of urinary stone diagnostics on the SLIPS-LAB. (**a-b**) The calibration of calcium detection and intensity difference of the RGB color elements at each concentration. (**c-d**) The calibration of uric acid detection and intensity difference of the RGB color elements at each concentration. (**e-f**) The calibration of citrate detection and intensity difference of the RGB color elements at each concentration. (**g-h**) The calibration of oxalate detection and intensity difference of the RGB color elements at each concentration. (**i-j**) The calibration of pH detection and intensity difference of the RGB color elements at each pH value.

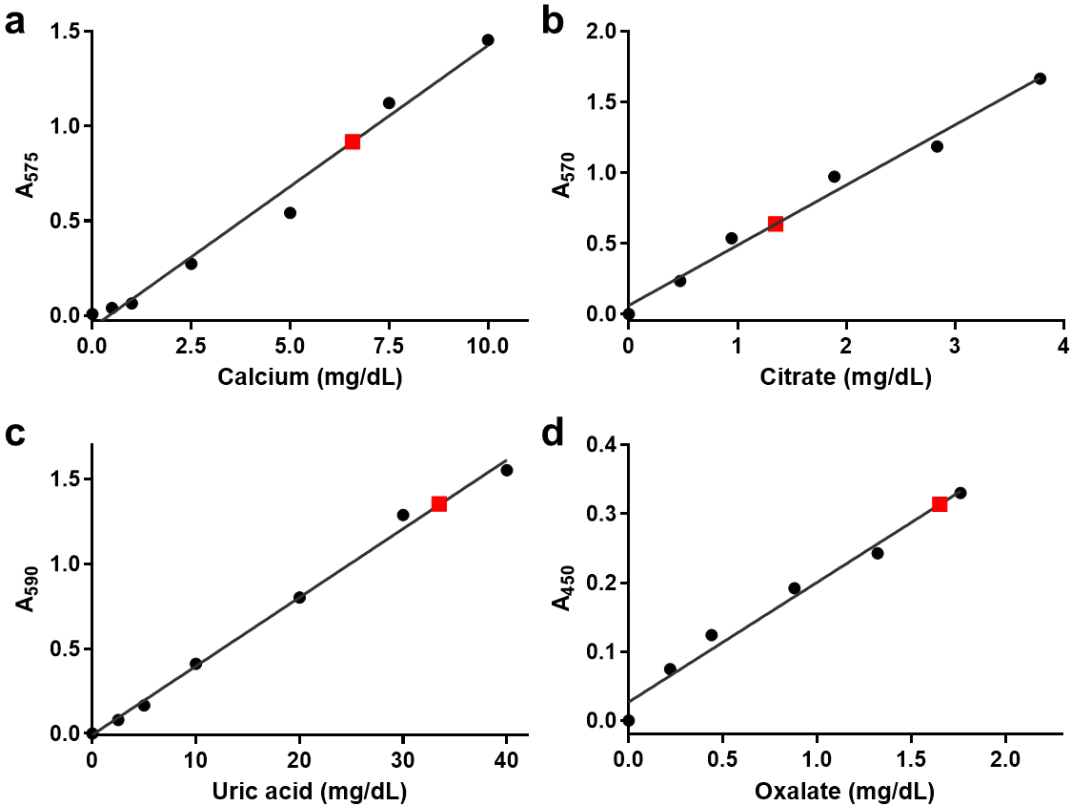

Figure S3-3. Calibration of urinary stone diagnostics using standard methods and corresponding testing for the volunteer's urine sample. (**a-d**) The calibration of calcium, citrate, uric acid, and oxalate detection at corresponding absorbance wavelength at each concentration. The red dots represent respective metabolic workups for the volunteer's urine sample.

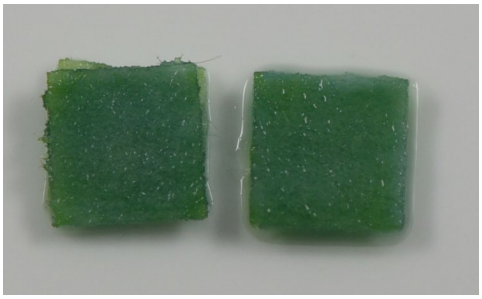

Figure S3-4. Detection of pH value for the volunteer's urine sample. Two pH stripes were used in the test and the pH values were estimated by the comparison with the reference color chart.

a

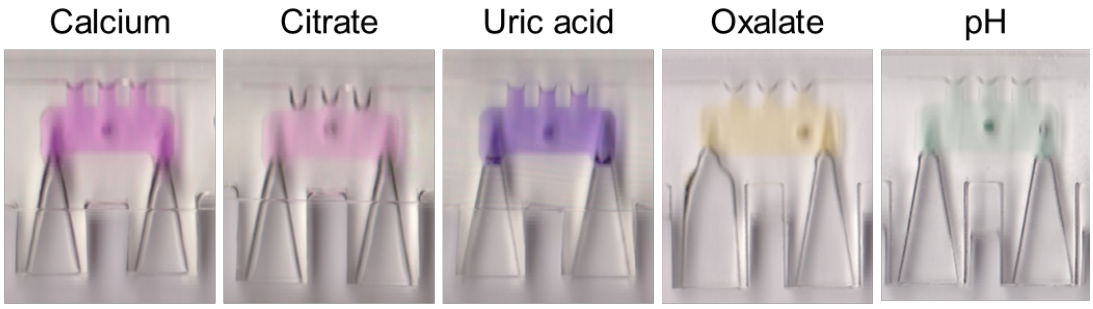

b

Parameters	Sensitive color	SLIPS-LAB (colar difference)			Calibration curves	Concentration from SLIPS-LAB (mg/dL)			Concentration from standard methods (mg/dL)
		#1	#2	#3		#1	#2	#3	
Calcium	Green	-42	-32	-36	y=-2.471x-0.7718	16.4	12.5	14.0	13.2
Citrate	Green	-21	-28	-33	y=-1.850x-0.767	11.0	14.8	17.7	13.6
Uric acid (*Diluted 2.5 times)	Green	-57	-68	-50	y=-1.76x-0.42	81.4	97.0	71.0	83.7
Oxalate (*Diluted 4 times)	Blue	-23	-24	-25	y=-12.70x-1.2	6.6	6.7	7.1	6.6
pH (*value)	Red	-32	-30	-26	y = -15.62x + 94.91	8.1	8.0	7.8	8.0

Figure S3-5. Detection of urinary stone related metabolic workups for the volunteer's urine sample using the SLIPS-LAB. (**a**) The scanning images of detecting calcium, citrate, uric acid, oxalate, and pH in the SLIPS-LAB, respectively. The images were representative for 3 independent assays. (**b**) The sensitive color element was examined and collected to calculate the concentration of the target.

Supplementary Table S3-1. pH buffer preparation using citric acid and disodium phosphate.

pH @ 22C	Ratio between the buffers (%)	
	Citric acid (0.1M)	Na_2HPO_4 (0.2M)
5.06	48.5	51.5
5.6	43.13	56.87
6.12	36.85	63.15
6.58	29	71
7.08	17.65	82.35
7.61	7.75	92.25
8.21	*TM buffer	

Supplementary Table S3-2. Mechanisms of the biochemical assays for testing critical urinary stone related metabolic workups.

Analytes	Normal range / critical concentration	Reaction/Purpose
Calcium	< 250 mg/day	Ca^{2+} + cresophthalein complexone $\xrightarrow{8-\text{Hydroxyquinoline}}$ **Complex**
Citrate	> 200 mg/day	Citrate $\xrightarrow{\text{Citrate lyase}}$ Oxaloacetate + acetate Oxaloacetate $\rightarrow$ pyruvate + CO_2 Pyruvate + phosphate + 0_2 $\xrightarrow{\text{Oxidase}}$ Acetyl phosphate + H_20_2 + CO_2 H_20_2 + ADHP $\xrightarrow{\text{HRP}}$ **Resorufin** + 2 H_20
Uric acid	< 800 mg/day	Uric acid + 2 Fe^{3+} $\rightarrow$ Compound I + 2 Fe^{2+} Fe^{2+} + 2 TPTZ $\rightarrow$ **$Fe(TPTZ)_2^{2+}$**
Oxalate	< 45 mg/day	Oxalate + H^+ $\xrightarrow{\text{Oxalate decarboxylase}}$ Formate + CO_2 Formate $\xrightarrow{\text{Enzyme}}$ Intermediate $\xrightarrow{\text{Probe}}$ **Complex**
pH	5.0 - 8.5	Colorimetric indicator including **methyl red** and **bromothymol blue**
Control	Ref	Optical control

Supplementary Table S3-3. Evaluation of the performance of the SLIPS-LAB for urinary stone diagnostics by comparing with the standard methods.

Parameters	SLIPS-LAB (mg/dL)	Standard method (mg/dL)	Error
Calcium	14.2	13.2	8%
Citrate	83.1	83.7	-1%
Uric acid	14.5	13.6	7%
Oxalate	6.8	6.6	3%
pH	8.0	8.0	0%

Appendix C

Supplementary materials for Chapter 4

Supplementary Table S4-1. Patient urine sample collection in the clinical study.

24hr patient urine for SLIPS-Lab		
ID	**Collect date**	**Volume (mL)**
1	9/18/2018	45
2	9/21/2018	42.5
3	9/21/2018	47.5
4	9/26/2018	42.5
5	9/26/2018	22.5
6*	9/28/2018	40
7*	10/3/2018	40
8	10/3/2018	47.5
9	10/5/2018	42.7
10	10/15/2018	40
11	10/16/2018	40
12	10/17/2018	40
13	10/23/2018	40
14	12/3/2018	NA
15	12/14/2018	40*2 tubes
16	1/16/2019	40*2 tubes

Supplementary Table S4-2. Sensitive color element changing and respective calculation in each assay to achieve the testing results for the patients' urine samples using the SLIPS-LAB.

Urinary stone diagnostics using the SLIPS-LAB											
Patient ID	Calcium, Green, y=-2.471x-0.7718		Citrate, Green, y=-1.85x-0.767		Uric acid, Green, y=-1.76x-0.42		Oxalate, Blue, y=-12.7x-1.2		pH, Red & green		
	Color	Conc. (mg/day)	Color	Conc. (mg/day)	Color	Conc. (mg/day)	Color	Conc. (mg/day)	Color (R)	Color (G)	pH value
1	-23	146	-18	280	-59	526	-17	38	1	-7	5.8
2	-4	17	-1	0	-54	407	-11	20	-5	-11	6.4
3	-16	117	-17	322	-53	572	-21	29	-30	-15	8.0
4	-10	112	-9	260	-41	699	-15	32	-4	-7	6.3
5	-49	225	-23	265	-38	487	-18	15	-1	-11	5.7
6	-45	632	-47	1653	-39	827	-21	53	-8	-9	6.6
7	-10	71	-30	533	-23	228	-16	42	2	-17	5.0
8	-1	0	-27	211	-72	317	-16	45	0	-14	6.2
9	-29	83	-14	98	-49	397	-11	28	-9	-13	6.7
10	-10	109	-19	510	-41	577	-10	55	0	-13	5.7
11	-23	98	-17	177	-30	179	-18	42	1	-12	5.4
12	-33	147	-39	440	-25	158	-20	49	3	-12	5.2
13	-17	180	-8	210	-43	679	-19	38	-8	-10	6.6
15	-20	229	-31	881	-65	1059	-17	71	0	-12	5.5
16	-25	234	-28	645	-53	696	-24	41	6	-8	5.7

VITA

HUI LI

EDUCATION AND PROFESSIONAL TRAINING

Pennsylvania State University PhD candidate, Biomedical engineering, Advisor: Prof. Pak Kin Wong	2015.08- present
University of Arizona PhD candidate, Mechanical engineering, Advisor: Prof. Pak Kin Wong	2014.09- 2015.08
MEMSIC Inc., Wuxi, China Senior sensor design engineer	2013.07- 2014.05
Peking University MS, Institute of Microelectronics, Advisor: Prof. Zhihong Li	2010.09- 2013.07
North University of China BS, Electronic Science and Technology	2006.09- 2010.07

PUBLICATIONS

[1] **Hui Li**, Peter Torab, Kathleen E. Mach, Christine Surrette, Matthew R. England, David W. Craft, Neal J. Thomas, Joseph C. Liao, Chris Puleo, and Pak Kin Wong. An Adaptable Microfluidic System for Single Cell Pathogen Classification and Antimicrobial Susceptibility Testing. ***Proceedings of the National Academy of Sciences of the United States of America***, 116 (21) 10270-10279, 2019.

[2] **Hui Li**, Tyler Garner, Francisco Diaz, and Pak Kin Wong. A Multiwell Microfluidic Device for Analyzing and Screening Non-Hormonal Contraceptive Agents, ***Small***, 2019, 1901910.

[3] **Hui Li**, Yi Lu, and Pak Kin Wong, Diffusion–reaction kinetics of microfluidic amperometric biosensors. ***Lab on a Chip***, doi:10.1039/C8LC00794B (2018).

[4] **Hui Li**, M. Morowitz, Neal J. Thomas, and Pak Kin Wong. Rapid Single Cell Microbiological Analysis – Toward Precision Management of Infections and Dysbiosis, SLAS Technology.

[5] Jian Gao*, **Hui Li***, Peter Torab, Kathleen E. Mach, David W. Craft, Neal J. Thomas, Chris M. Puleo, Joseph C. Liao, Tza-Huei Wang, and Pak Kin Wong, Nanotube Assisted Microwave Electroporation for Single Cell Pathogen Identification and Antimicrobial Susceptibility Testing, ***Nanomedicine: Nanotechnology, Biology, and Medicine***, 17, 246-253, 2019. (*Co-first authors)

[6] Gloria B. Kim, Yongjie Chen, Weibo Kang, Jinshan Guo, Russell Payne, **Hui Li**, Qiong Wei, Julianne Baker, Cheng Dong, Sulin Zhang, Pak Kin Wong, Elias B. Rizk, Jiazhi Yan, Jian Yang, The critical chemical and mechanical regulation of folic acid on neural engineering, ***Biomaterials***, 178, 504-516, 2018.